

University of Windsor

## Scholarship at UWindor

---

Electronic Theses and Dissertations

Theses, Dissertations, and Major Papers

---

2008

### Fault tolerant control for an electric power steering system

Matthew Lawson  
*University of Windsor*

Follow this and additional works at: <https://scholar.uwindsor.ca/etd>

---

#### Recommended Citation

Lawson, Matthew, "Fault tolerant control for an electric power steering system" (2008). *Electronic Theses and Dissertations*. 7945.

<https://scholar.uwindsor.ca/etd/7945>

This online database contains the full-text of PhD dissertations and Masters' theses of University of Windsor students from 1954 forward. These documents are made available for personal study and research purposes only, in accordance with the Canadian Copyright Act and the Creative Commons license—CC BY-NC-ND (Attribution, Non-Commercial, No Derivative Works). Under this license, works must always be attributed to the copyright holder (original author), cannot be used for any commercial purposes, and may not be altered. Any other use would require the permission of the copyright holder. Students may inquire about withdrawing their dissertation and/or thesis from this database. For additional inquiries, please contact the repository administrator via email ([scholarship@uwindsor.ca](mailto:scholarship@uwindsor.ca)) or by telephone at 519-253-3000ext. 3208.

# NOTE TO USERS

This reproduction is the best copy available.

**UMI**®



**Fault Tolerant Control**  
for an  
**Electric Power Steering System**

By  
**Matthew Lawson**

A Thesis  
Submitted to the Faculty of Graduate Studies  
through Electrical and Computer Engineering

in Partial Fulfillment of the Requirements for  
the Degree of Master of Applied Science at the  
University of Windsor

Windsor, Ontario, Canada

2008

© 2008 Matthew Lawson



Library and  
Archives Canada

Published Heritage  
Branch

395 Wellington Street  
Ottawa ON K1A 0N4  
Canada

Bibliothèque et  
Archives Canada

Direction du  
Patrimoine de l'édition

395, rue Wellington  
Ottawa ON K1A 0N4  
Canada

*Your file* *Votre référence*  
*ISBN: 978-0-494-47090-9*  
*Our file* *Notre référence*  
*ISBN: 978-0-494-47090-9*

#### NOTICE:

The author has granted a non-exclusive license allowing Library and Archives Canada to reproduce, publish, archive, preserve, conserve, communicate to the public by telecommunication or on the Internet, loan, distribute and sell theses worldwide, for commercial or non-commercial purposes, in microform, paper, electronic and/or any other formats.

The author retains copyright ownership and moral rights in this thesis. Neither the thesis nor substantial extracts from it may be printed or otherwise reproduced without the author's permission.

---

In compliance with the Canadian Privacy Act some supporting forms may have been removed from this thesis.

While these forms may be included in the document page count, their removal does not represent any loss of content from the thesis.

#### AVIS:

L'auteur a accordé une licence non exclusive permettant à la Bibliothèque et Archives Canada de reproduire, publier, archiver, sauvegarder, conserver, transmettre au public par télécommunication ou par l'Internet, prêter, distribuer et vendre des thèses partout dans le monde, à des fins commerciales ou autres, sur support microforme, papier, électronique et/ou autres formats.

L'auteur conserve la propriété du droit d'auteur et des droits moraux qui protègent cette thèse. Ni la thèse ni des extraits substantiels de celle-ci ne doivent être imprimés ou autrement reproduits sans son autorisation.

---

Conformément à la loi canadienne sur la protection de la vie privée, quelques formulaires secondaires ont été enlevés de cette thèse.

Bien que ces formulaires aient inclus dans la pagination, il n'y aura aucun contenu manquant.



# Canada

## DECLARATION OF PREVIOUS PUBLICATION

This thesis includes [2] original papers that have been previously published/submitted for publication in peer reviewed conferences, as follows:

Thesis Chapter	Publication title/full citation	Publication status*
Chapter 3	<i>"Fault Tolerant Control for an Electric Power Steering System"</i> ; 2008 MSC IEEE Multi-Conference on Systems and Control, San Antonio, Texas, Sept. 2008	published
Chapter 3,4	<i>"Hardware-in-the-Loop Simulation of Fault Tolerant Control for an Electric Power Steering System"</i> ; 2008 VPPC Conference, Harbin, China, Sept. 2008	published

I certify that I have obtained a written permission from the copyright owner(s) to include the above published material(s) in my thesis. I certify that the above material describes work completed during my registration as graduate student at the University of Windsor.

I declare that, to the best of my knowledge, my thesis does not infringe upon anyone's copyright nor violate any proprietary rights and that any ideas, techniques, quotations, or any other material from the work of other people included in my thesis, published or otherwise, are fully acknowledged in accordance with the standard referencing practices. Furthermore, to the extent that I have included copyrighted material that surpasses the bounds of fair dealing within the meaning of the Canada Copyright Act, I certify that I have obtained a written permission from the copyright owner(s) to include such material(s) in my thesis.

I declare that this is a true copy of my thesis, including any final revisions, as approved by my thesis committee and the Graduate Studies office, and that this thesis has not been submitted for a higher degree to any other University of Institution.

## **ABSTRACT**

Electric power steering (EPS) systems are rapidly replacing existing traditional hydraulic power steering systems due to fuel and cost savings. The reliability of a column mounted EPS is improved by adding an alternate control scheme that is tolerant to a torque sensor failure (FTC). To accomplish this, a motor model based observer is used to estimate the total torque on the motor shaft. An independent estimate of the road reaction torque is generated from vehicle navigation signals and subtracted from the total to estimate the torque sensor output. A Hardware-in-the-loop (HIL) simulation is described where the EPS model, road vehicle dynamics and developed control scheme are simulated on an Opal RT™ real-time platform and a physical DC motor is placed in-the-loop. This simulation validates the developed method under more realistic operating conditions than using software simulation alone and is more repeatable and cost effective than a full in-vehicle test.

## DEDICATION

*My wife, who is my soul mate and the reason I completed this endeavor*

*My Parents, for their constant, loving support*



## **ACKNOWLEDGEMENTS**

I would like to express my sincere gratitude to my advisor Dr. Xiang Chen, for his guidance and patience throughout the course of this work.

I would also like to thank Dr. N. Kar, Dr. M. Ahmadi and Dr. M. Sid-Ahmed for their suggestions and support during my stay at the University of Windsor.

My thanks go to Mr. Frank Cicchello and Mr. Don Tersigni, for their technical support throughout my research.

Finally, I would like to acknowledge the greatly appreciated financial support provided by the Natural Sciences and Engineering Research Council (NSERC).

# TABLE OF CONTENTS

DECLARATION OF PREVIOUS PUBLICATION.....	iii
ABSTRACT.....	iv
DEDICATION.....	v
ACKNOWLEDGEMENTS.....	vi
LIST OF FIGURES.....	ix
LIST OF TABLES.....	ix
NOMENCLATURE.....	x
ABBREVIATIONS.....	xii
NOTATION.....	xiii
<b>CHAPTER</b>	
<b>1. INTRODUCTION</b>	
1.1 EPS Overview.....	2
1.2 Literature Survey.....	3
1.3 Thesis Outline.....	9
<b>2. MODELS AND PRELIMINARY THEORY</b>	
2.1 DC Motor Model.....	10
2.2 Torque Sensor.....	11
2.3 EPS Control Model.....	13
2.4 Vehicle and Tire Dynamics.....	16
2.5 Observer Theory.....	21
<b>3. DESIGN AND METHODOLOGY</b>	
3.1 Estimating Shaft Torque via Motor Model Based Observer.....	25
3.2 Estimating Road Torque from Vehicle and Tire Dynamics.....	37
3.3 FTC of EPS by combining previous methods.....	41
<b>4. HIL SIMULATION SETUP AND ANALYSIS</b>	
4.1 Overall Topology.....	44
4.2 Drive Topology for EPS Motor and Dynamometer.....	47
4.3 Controller and Simulation Specifics.....	50
4.4 FTC implementation.....	53
4.5 Determining Motor and Simulation Parameters.....	55
4.6 Analyzing the Effect of Parameter Variations on FTC Scheme.....	57

4.7	Results .....	61
<b>5.</b>	<b>CONCLUSIONS AND FUTURE WORK</b>	
5.1	Conclusions .....	67
5.2	Future Work .....	68
<b>APPENDICES</b>		
A.	Glossary of Model Parameters and Control Variables.....	71
<b>REFERENCES.....</b>		<b>72</b>
<b>VITA AUCTORIS .....</b>		<b>77</b>

## LIST OF FIGURES

Figure 1.1: EPS illustrated Description .....	2
Figure 2.2: DC Motor Torque Control using PI law.....	10
Figure 2.3: Optical Torque Sensor.....	12
Figure 2.4: Magneto-Restrictive Torque Sensor.....	12
Figure 2.5: Column mounted EPS system, model overlaid.....	13
Figure 2.6: EPS Control Model .....	14
Figure 2.7: Tire Deformation (Causing lateral force) versus slip angle .....	17
Figure 2.8: Planar Bicycle Model .....	18
Figure 2.9: Rolling Tire Deformation and Lateral Force.....	20
Figure 2.10: Observer viewed as a Feedback system .....	23
Figure 3.11: DC Motor Subsystem of an EPS system.....	25
Figure 3.12: EPS Torque Sensor FTC Scheme.....	42
Figure 4.13: EPS HIL Simulation Model Based Description.....	44
Figure 4.14: Alternate Motor Drive Topology .....	47
Figure 4.15: External Torque Balance Block .....	50
Figure 4.16: PI Control Logic.....	51
Figure 4.17: Hardware and Software Configuration for FTC of EPS .....	53
Figure 4.18: Block Diagram of FTC HIL Simulation setup .....	54
Figure 4.19: Frequency and Step Response of EPS subject to parametric variations .....	58
Figure 4.20: Comparison of FTC to standard controller.....	63
Figure 4.21: Normal EPS Controller - HIL Performance .....	64
Figure 4.22: EPS FTC - HIL Performance, Nominal Observer Parameters.....	65
Figure 4.23: FTC Performance, 20% parameter variation .....	66
Figure 4.24: FTC Performance, Increased Road Roughness.....	66

## LIST OF TABLES

Table 3.I: Frequency of Road Information .....	39
Table 4.II: Determining Motor and Other Simulation Parameters .....	55
Table 4.III: Summary of Experimental Assumptions and Settings .....	61

## NOMENCLATURE

$\alpha_f$	Vehicle tire slip angle
$\beta$	Vehicle slip angle
$\mu$	Tire-road friction coefficient
$\delta$	Vehicle front steering angle
$\theta_m, \theta_p$	Motor, pinion angular position
$\omega_m, \omega_p$	Motor, pinion angular velocity
$\psi$	Vehicle yaw angle
$\gamma$	Direction of velocity (heading)
$a_y, a_x$	Vehicle longitudinal/lateral acceleration (at center of gravity)
$a$	Distance from front tire to vehicle center of gravity
$b$	Distance from rear tire to vehicle center of gravity
$B_m, B_{rp}$	Motor, rack and pinion viscous friction
$C_1$	Motor torque controller (PI)
$C_2$	Robust torque shaping controller
$C_\alpha$	Effective front cornering stiffness
$e_{signal}$	Error between actual and estimated signal
$F_{y/f/r}$	Front / Rear lateral tire forces
$G$	Steering assist gain
$h_{LPF}$	Transfer function of the low pass filter
$i_a$	Motor armature current
$I_z$	Vehicle moment of inertia about yaw axis
$J, B$	Inertia and dampening of handwheel shaft
$J_{eq}, B_{eq}$	Equivalent inertia/ viscous friction on pinion axis
$J_m, J_{rp}$	Motor, rack and pinion inertia
$K$	Motor flux constant, $K=K_t=K_e$
$K_i$	Integral gain of torque controller
$K_f$	Coulomb friction constant
$K_p$	Proportional gain of torque controller
$K_s, B_s$	Spring and dampening constant of torque sensor

$L_a$	Motor armature inductance
$m$	Vehicle mass
$n, n_g$	Motor gearbox ratio
$n_s$	Vehicle effective steering ratio
$\rho_i$	Motor model parameters used by observer
$r$	Vehicle yaw rate
$R_a$	Motor effective armature resistance
$R_s$	Sense resistor used for current feedback
$R_{ts}$	Residual signal used for fault detection
$V_t$	Motor terminal voltage
$T_{align}$	Aligning component of road torque
$T_d$	Total motor shaft load/disturbance torque
$T_f$	Coulomb friction torque
$T_i$	H-Bridge power transistors
$t_m$	Tire Mechanical trail
$t_p$	Tire Pneumatic trail
$T_{road}$	Road reaction torque
$T_{ts}$	Torque sensor voltage signal / torsion bar torque
$V_y, V_x$	Vehicle longitudinal/lateral velocity at center of gravity

## ABBREVIATIONS

ABS	Anti-lock Braking System
CAN	Controller Area Network
DC	Direct Current
DSP	Digital Signal Processor
DOB	Disturbance Observer
DOF	Degree of Freedom
EMF	Electro Motive Force
EMI	Electromagnetic interference
EPS	Electric Power Steering
ESP	Electronic Stability Program
FDI	Fault Detection and Isolation
FTC	Fault Tolerant Control
GIMC	Generalized Internal Model Control
GPS	Global Positioning System
HIL	Hardware-in-the-Loop
HSRI	Highway Safety Research Institute
INS	Inertial Navigation System
I/O	Input / Output
LTI	Linear Time Invariant
ODE	Ordinary Differential Equation
O/S	Operating System
PID	Proportional Integral Derivative
PWM	Pulse Width Modulation
SISO	Single Input, Single Output
SNR	Signal to Noise Ratio
VSC	Vehicle Stability Control

## NOTATION

$u$             *Italicized* characters represent a variable, parameter, or a vector of these

**B**            **Bold** characters represent a matrix of variables or parameters

$\hat{x}$             ^ indicates the variable contains an estimated value

$\dot{x}$             Indicates the derivative

$\int$             Integral; indefinite



# CHAPTER 1

## INTRODUCTION

Fault management in a controlled process is perhaps as important as the main control algorithms. A system equipped with FDI (Fault Detection and Isolation) techniques senses when a fault is about to or has just occurred, and takes an appropriate action to prevent the fault from negatively influencing the system performance. For example, it may be possible to maintain system stability and preserve functionality; in other cases, it may be necessary to shut down the system entirely. FTC (Fault Tolerant Control) allows the system to retain functionality despite a fault, but perhaps at somewhat degraded performance.

In this thesis, FTC for the torque sensor of an EPS (Electric Power Steering) system is explored. The torque sensor voltage output determines the torque command to the EPS motor drive, and it is relatively the most complex sensor. Thus, adding techniques to maintain system function despite a fault or failure in this sensor significantly increases the reliability of the overall system.

In the following sections, background in EPS and related state of the art applications are surveyed. The ultimate target is to tolerate a torque sensor failure using only other measurable signals already available. In this way, no additional cost is added, which is paramount in the cost driven automotive industry. Hence, the subsequent sections of the survey explore disturbance estimation methods used in motor drives and in other vehicle control systems which are already available.

## 1.1 EPS Overview

In conventional electric power steering, the torque sensor is used to estimate the driver's torque, and the motor torque follows this signal. As the motor, through the gearbox, delivers a larger share of the steering effort, the wheels become easier to turn. This steering assist motor torque is generated by comparing the torque sensor signal with feedback of the motor armature current. For a fixed field or permanent magnet DC motor, the armature current is directly proportional to the electromagnetic torque in the linear magnetic operating region of the motor. The overall configuration is shown in *Figure 1.1*. Further analysis and insight into an EPS system can be found in [1].

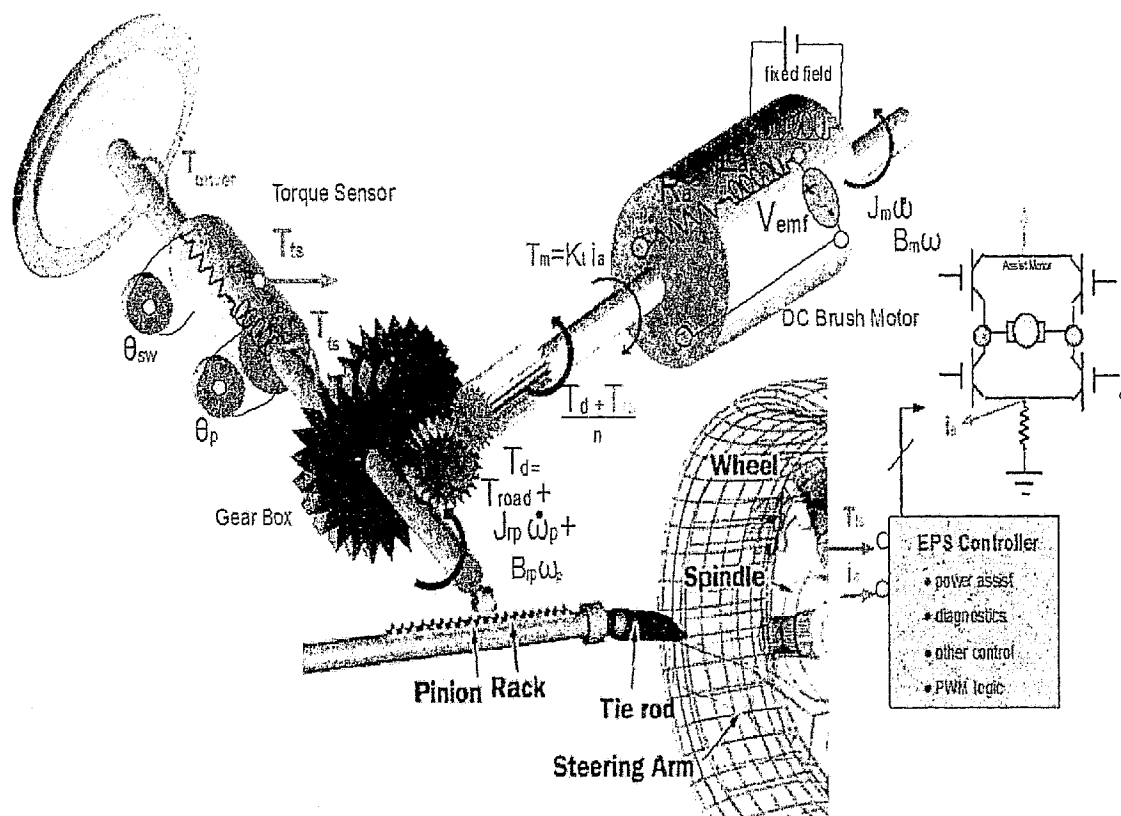


*Figure 1.1: EPS illustrated Description*

## 1.2 Literature Survey

### **EPS Control Applications**

Besides providing the steering assist function previously described, the EPS controller also provides other functions and diagnostics. For instance, the steering assist gain, which is the gain from driver's torque (indicated by the torque sensor output) to the motor torque, is varied depending on the vehicle speed. At lower speeds, more steering assist is available to aid in parking and maneuvering; likewise, at high speeds, the gain is lowered to improve the driver's feel of the road and maintain vehicle stability.

The signals used by a typical EPS system (torque sensor, current sensor) can also be incorporated into other vehicle control systems. Firstly, the steering torque and steering angle delivered by the torque sensor can be used as inputs to vehicle control and estimation schemes. An example is the application of steering torque to vehicle state estimation, see [3]. Many control methods are being developed for the SBW (steer-by-wire) system; however, an EPS equipped with a torque sensor can use motor signals to deliver an accurate estimate of the road torque, as will be detailed later. This road torque can be used in a similar manner as the steering torque is used in a SBW system. As well, since the EPS controller is integrated with the rest of the vehicle controllers through a CAN, the EPS motor can be used as an actuator in VSC systems in conjunction with ABS. These systems control/limit the vehicle yaw rate and slip angle, see [4].

More advanced control techniques and algorithms can be used to improve the perceived performance felt by the driver. To reduce rough road torques (that are transferred from the road to the steering wheel) felt by the driver,  $H_2/H_\infty$  control techniques can be employed to generate a torque demand which penalizes the higher frequency torques generated by uneven and rough road surfaces, while maintaining the lower frequency road reaction torque. This is crucial since it indicates road grip and perceptual feedback to the driver [5]. Better return to center performance can be accomplished using the

steering wheel position signal or using static steering control as in [6]. Knowledge of the wheel position also allows active dampening to reduce oversteer and understeer [7].

In addition to improving the steering performance, maintaining driver feel, and integration into other vehicle control systems, the EPS controller should include fault diagnosis and fault tolerant methods to improve the safety of the vehicle, as in [8,9]. Besides the brake system, the steering system is the most critical manner in which a vehicle is controlled by the driver, and thus must be maintained if at all possible. Furthermore, driving an EPS system in manual mode is more difficult than a manual steering system due to the additional inertia added by the motor rotor through the gearbox. This could be problematic to how quickly the driver could respond, especially in large vehicles when the power assist system fails.

One way to manage faults in control systems is tolerating them by including additional backup actuator and/or sensors and choosing the non-faulted ones through a polling system, see [9]. In [10], a FTC scheme is developed by adding multiple actuators (motors) that can work in parallel or alone. However, redundant hardware adds significant cost and weight to the vehicle. For sensors such as the torque sensor, which add compliance to the steering shaft, it is impractical to add a redundant sensor. Hence, methods introduced in this thesis manage faults in a different manner. In this case, a torque sensor failure is tolerated by employing analytic redundancy: estimates of the faulted sensor are obtained using knowledge of the plant model and other sensor signals.

### **Motor Torque Disturbance Estimation and Compensation**

Motor drives themselves include sensor signals (current, angular speed and position) which can be used to detect, diagnose, and compensate for both hard (i.e. sensor failure) and soft (i.e. sensor drift, component wear) faults that can potentially occur in the motor. In [11], 14 different faults are diagnosed in a DC motor drive using measurements of input voltage, angular speed, and armature current. This paper uses a set of motor parity equations, the deviation of the system from its model, as fault indicators. Additional fault indicators include estimates of the motor parameters. These are used to generate

residual signals (i.e. by comparing a parameter estimate to its nominal value). A neuro-fuzzy scheme takes these fault indicators and determines which fault or failure has occurred. The disadvantage for this scheme to extend to the EPS case is that the load torque must be known; the EPS motor drive is subject to relatively unknown load torques generated from the road and driver. In [12], the author uses a Block-Pulse Function Series parameter estimation scheme to diagnose 8 motor physical faults, including brush wear. In [13], even multiple simultaneous sensor faults are tolerated by constructing a virtual compensated signal for each of the system's 3 sensors: the motor position, shaft speed, and robotic arm deflection. Incipient faults, slow occurring faults and total failures are compensated for.

Different estimation schemes can be used to tolerate faults in systems with similar models. Some methods perform better depending on the nature of intended system and measurements available. For example, in some systems sensor noise is significant; in other systems, unknown inputs or non-linearity are significant. In [15], a FTC scheme is designed for a speed sensor fault in a DC motor drive using sliding mode observers. These observers use the predictor/corrector filter structure, while adding an additional time varying term to improve the accuracy of the estimated signals. These time-varying terms can account for unknown system disturbances and non-linearity, but result in a chattering problem, especially for noisy sensors. In [16], the same is accomplished using  $H_2/H_\infty$  techniques and the GIMC structure. In [18], a detailed comparison between sliding mode, classical, and nonlinear extended Luenberger and Kalman observers is presented, in context of their usage in FDI and FTC. For most systems with significant plant uncertainty and external disturbances, non-linear extended state observers tend to fair better than their high gain classical and sliding mode counterparts, since robustness to these issues are inherent in their structure.

Different methods can be used to estimate and compensate for disturbances. One such method is by calculating the disturbance directly from the system model, state and input measurements. This is called a DOB, see an example in [17]. A DOB's performance is proportional to the low pass Q filter's cutoff frequency and roll-off rate. This model

based calculation would be prone to any error in the nominal motor parameter measurements and require measurement of all the system states. However, when the torque/angle sensor is faulted in an EPS system, there is no other measurement of angular speed  $\omega_m$ . Even calculating  $\omega_m$  using  $\theta_m$  (typically measured with low resolution hall-effect sensors for brushless motor commutation) would be insufficient to calculate the inertial term. If another position or speed sensor were available in the EPS unit, DOB designs, as in [35], would work well to estimate  $T_L$  and reduce errors caused by plant parameter variations.

Other disturbance compensation schemes employ the DOB but improve its performance with adaptive techniques. In [24] a so called reaction force observer is used to compensate for a faulted strain gauge sensor in a flexible robot arm. This scheme utilizes a DOB observer to estimate the strain signal from the applied motor torque and motor angle. Increased robustness to parameter variations is accomplished by introducing a least squares adaptive gain that is only updated when the system is fault free (the strain gauge is available).

Another approach for disturbance estimation and compensation is the use of augmented observers [3,36] or colored noise Kalman filters [34]. In both of these approaches, the disturbance is modeled as slowly varying or of low frequency compared to the system's states. In this way, the addition of a disturbance adds an extra dimension to the augmented system model but does not affect the observability. The actual filter gains (which determine how greatly weighted the measurements are compared to values predicted by the system model) can be determined using a variety of techniques. Different methods of designing the filter gains use different performance criteria, and result in estimates that meet different objectives: the  $H_2$ /Kalman filter (optimal, minimizes the average error), Luenberger observer (pole placement, determines the speed of error convergence),  $H_\infty$  (robust, minimizes the worse case error), sliding mode observers (handles non-linearity better by adding additional time-varying corrector terms), and non-linear variations of these.

## Road Torque Estimation

As a DC motor has a linear system description, many of the previously discussed and similar techniques could be applied to the EPS to obtain the applied torque on the motor shaft. The question then becomes how to distinguish between the different external disturbances on the motor shaft. The EPS system interacts with the motor by reflecting onto it both the torque due to the torque sensor (indicates driver torque, what is to be estimated) and the opposing road torque from the tire / road interaction. Hence, the approach taken in the thesis necessitates estimating the low frequency, aligning component of the road torque, as well as the total applied torque.

In fact, when the torque sensor is operating correctly, the road torque can be estimated from the EPS motor signals. This can be accomplished by estimating the total applied torque on the motor and then subtracting out the amount from the torque sensor, which is measured. This road torque can be used for many applications. For example, in [3], this torque is used to better estimate a main vehicle parameter used in vehicle control systems, the slipside angle  $\beta$ . Although the slipside angle is observable using vehicle models and measuring yaw rate, the system becomes unobservable as the system approaches neutral steering. This is where the additional equations from the motor come in to play, making the system observable under all driving conditions. As well, this motor based road torque estimate could be used to reduce steering wheel vibrations, as in [19]. The road torque signal is high pass filtered to obtain the undesired rough road torque component and is directly compensated for by applying a motor torque equal but opposite in direction. A motor with a small electrical time constant can develop torque quickly, and would be able to more effectively cancel the effects of higher frequency vibrations in this case.

To be able to estimate the torque sensor signal with no additional hardware, an independent estimate of the road torque is needed. In [20], the road torque is determined by first estimating the tire slipside angle, which can then be used to calculate the road torque from tire models. The author uses an INS for 100 Hz sampled velocities and yaw rates. Since the velocities and yaw rates are obtained from integrating accelerometer and

gyroscope measurements, they are prone to integration drift. To compensate for this drift, these values are updated using 5 Hz GPS signals, which measure the velocities and yaw rates directly. Note that the GPS signal itself would not have sufficient bandwidth for control applications. This technique is demonstrated on a test vehicle, showing it to provide reasonable results. Many different techniques can be used to estimate the vehicle slippage angle. Reference [21] compares different observer techniques (linear, extended state, and sliding mode) using different sets of sensors. As well, the assumption of a constant cornering stiffness [20] is shown to be less valid as the speed of the vehicle increases.

In [22], the vehicle-road contact parameters (cornering stiffness and tire/road friction coefficient) are estimated in real-time. These parameters can be used to calculate the road torque from estimated slippage angle, as in [20]. Non-linear least squares fitting techniques are applied to the tire dynamics modeled with the HRSI model [23]. This has the added benefit of being able to determine the tire/road contact friction coefficient earlier, before the tires reach their maximum grip. This could result in future vehicle control systems being able to stabilize a vehicle before the driver starts to lose control. This method uses information from a motor based disturbance observer in a Steer-by-Wire system. Since there is no mechanical connection to the steering wheel, the total applied torque delivered by a motor observer is an estimate of the road torque only. This method could be extended in a similar manner to an EPS system by subtracting out the torque sensor signal from the total applied torque. Under torque sensor fault free condition the vehicle parameters can be continuously updated. If a torque sensor failure occurs, the most recent parameter estimates could be used. In this way, when the torque sensor fails the road torque can be more accurately estimated from slippage angle, resulting in a better torque sensor estimate. Moreover, if the cornering stiffness is considered slowly varying, than it can be updated simultaneously with the road torque estimate. Such as method using least squares techniques can be found in [24].



### 1.3 Thesis Outline

This thesis is structured as follows: in Chapter 2, the relevant control models and preliminary theory required for the methods in Chapter 3 are detailed. Moreover, methods of state estimation and relevant vehicle handling dynamics are detailed.

In Chapter 3, the main methodology to address fault tolerant control for a torque sensor is provided. This includes how to estimate the torque sensor signal from a combination of a motor model based disturbance observer and an independent estimate of the tire aligning moment.

In Chapter 4, methods are presented to test the standard and fault tolerant controllers using a Hardware-in-the-Loop (HIL) simulation. A HIL simulation provides a balance between cost/flexibility/repeatability of the experiment (versus an in vehicle test) and realism (versus a software only simulation). HIL results are presented and analyzed.

Finally, Chapter 5 summarizes the results and makes recommendations for further research.

## CHAPTER 2:

# MODELS AND PRELIMINARY THEORY

### 2.1 DC Motor Model

Figure 2.2 presents a DC motor with the model of the armature winding electrical dynamics and shaft load dynamics overlaid. This is the model that will be used to develop the observers and control systems in the subsequent chapters. Figure 2.2 also shows how the torque is controlled: by feedback of the current through the armature windings, measured with a small series resistor. Due to the current smoothing effects of the armature winding inductance, PWM (pulse-width modulation) techniques can be employed, typically with an H-Bridge configuration, to vary the average voltage of the motor using a fixed power supply. The command voltage is generated by a PI controller, with the torque sensor as the input signal and using the armature current as the feedback signal, in order to control the steering assist torque.

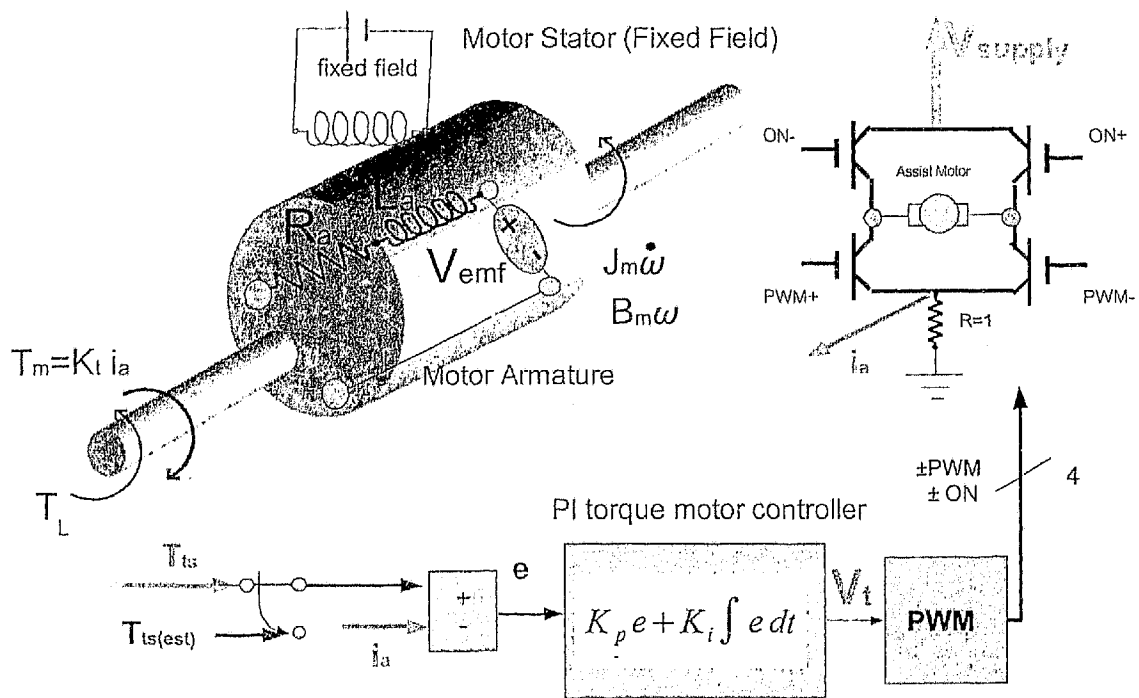


Figure 2.2: DC Motor Torque Control using PI law

## 2.2 Torque Sensor

The torque sensors typically used in EPS applications are based on the torsion bar principle: the amount of twist of the bar between the lighter (driver) and heavier load side end (EPS motor / rack and pinion assembly) indicates primarily the driver's instructional torque. This twist, or angular difference, is measured through either optical [26] encoders or magnetic sensing methods, see [27]. As well, contact-less torque sensors are available, but are typically used for higher end vehicles where rack mounted EPS are used [8]. As torque sensors are measuring various physical quantities instead of one electrical one (the sense resistor), they are the most fault prone in the EPS system.

Two different configurations are shown in the following two figures. *Figure 2.3* shows a configuration which measures the torsion torque by measuring the angular position of each end of the shaft via an optical encoder, and uses pulleys to increase the effective angular resolution [28]. *Figure 2.4* shows a configuration using a resistive element substrate; like a potentiometer, the change in resistance can be used to output a voltage proportional to twist in the torsion bar [26].

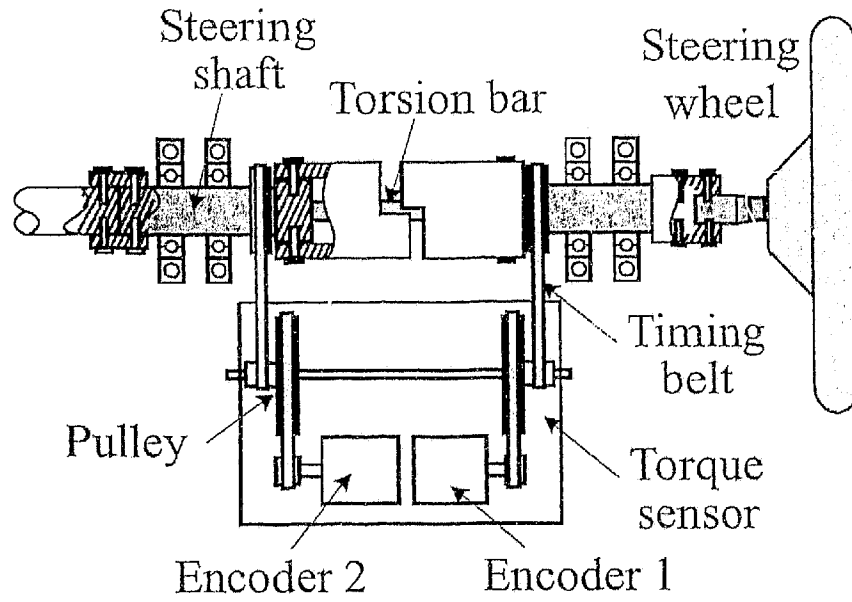


Figure 2.3: Optical Torque Sensor

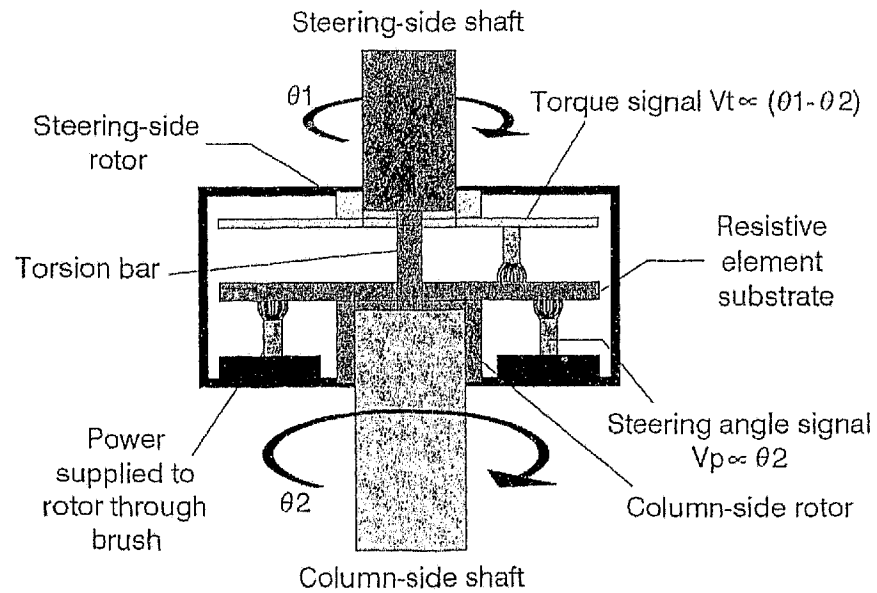
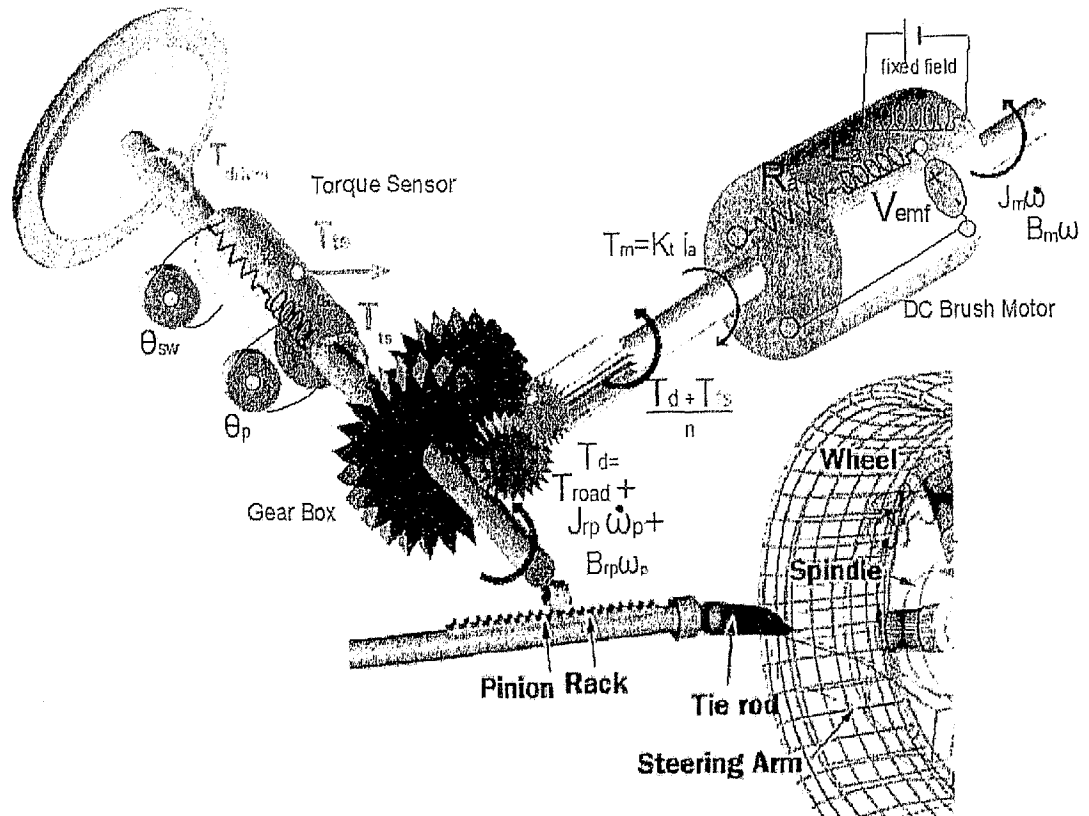


Figure 2.4: Magneto-Restrictive Torque Sensor

### 2.3 EPS Control Model

A full detailed mathematical derivation of the EPS model can be found in [24]. This section of the thesis will explain the individual and connective dynamics of the EPS system (steering column, torque sensor, motor, gearbox, and rack and pinion connection). The relevant equations will be detailed in Chapter 3. The overall physical configuration with the motor and torque sensor model overlaid is shown below in *Figure 2.5*.



*Figure 2.5: Column mounted EPS system, model overlaid*

The methods used in this thesis are intended for linear systems. No real physical system is truly linear, but often the non-linear dynamics are insignificant enough to neglect. On that note, the following assumptions are made regarding the EPS model:

## Model Assumptions

### Mechanical dynamics

- All shafts and connectivity are assumed rigid
- Dry (Coulomb) and other non-linear friction are ignored in the models. However, dry friction compensation is added in the HIL simulation of Chapter 4.
- Torque sensor voltage output is assumed perfect
- The non-linear road-tire contact dynamics are considered a disturbance input

### DC Motor dynamics

- Brush / commutator effects neglected
- Ideal gearbox (100% efficiency and ignores teeth backlash)
- Armature reaction effect ignored in case of wound field with compensated windings
- Non-linear magnetic effects ignored in case of permanent magnet field
- Magnetic saturation neglected
- Torque ripple caused by commutation ignored (as a motor with a large number of poles is used)

Neglecting the above effects the model describing the EPS system is linear. Many of the non-linear effects are minimal or can be compensated for individually. The linear control-oriented system model is shown in *Figure 2.6*. Since the physical parameters change much slower than the dynamic states, the model is also LTI.

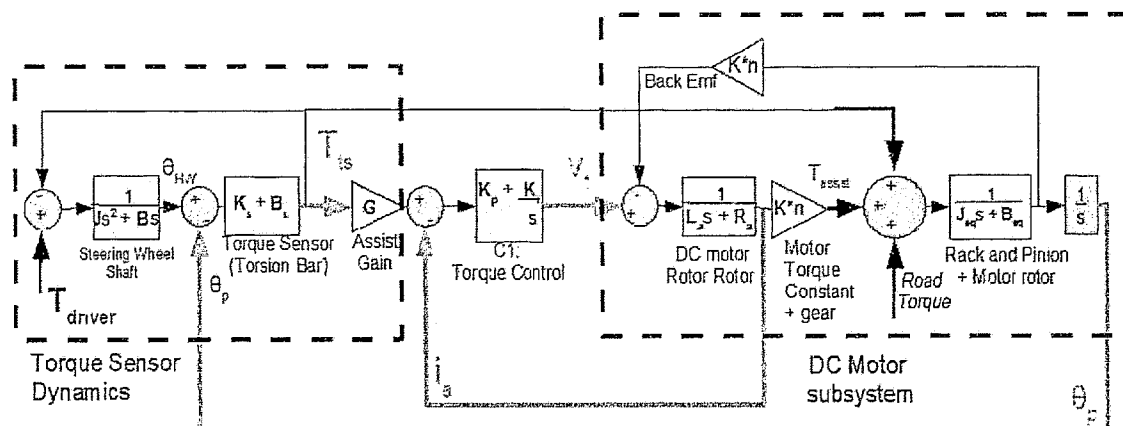


Figure 2.6: EPS Control Model

The driver applies torque  $T_{driver}$  to the steering shaft, which rotates with an angle  $\theta_{HW}$  and is connected to the 1<sup>st</sup> end of the torsion bar. The torsion bar has stiffness  $K_s$ , which is the mechanical component of the torque sensor. The torsion bar twists upon an external torque being applied, and responds with a torque  $T_{ts}$ , which is proportional to angular difference of its two ends (steering side  $\theta_{HW}$  and pinion side  $\theta_p$ ). This torsion torque is applied back onto the steering shaft and onto the pinion axis, as well as onto the motor shaft through the gearbox. The rotational motion of the pinion shaft is converted to linear motion via the rack and pinion connection, which is translated to the wheels via the tie rod and steering arm.

The motor interacts with steering system by assisting the driver's instructional torque. The driver's torque is represented by the torsion bar torque, which is measured by the torque sensor. The motor applies a torque equal to the torque sensor output multiplied by the steering assist gain  $G$ . This motor command signal may be low-pass filtered to remove noise from the road and sensor signal. The motor torque is applied onto the pinion shaft, leveraged by the gearbox ratio  $n$ . A controller  $C_2$ , in the same location as the gain  $G$ , can be used to remove rough road noise by shaping the desired torque, see [39, 40].

The road/tire interaction results in lateral forces applied onto the rack, creating an aligning moment and other torque components on the pinion shaft. The details of this will be explained in *Section 3.2*; in simulation, these dynamics are provided by CarSim<sup>TM</sup>.

The output of the controller  $C_2$  (in this study it is equal to  $G$ ) is input to a motor torque controller  $C_1$ . The function of this controller is to cause the electromagnetic assist torque to accurately and quickly follow this command, ideally with no overshoot.

## 2.4 Vehicle and Tire Dynamics

As only the total torque applied on the motor shaft can be estimated from motor information alone, an independent estimation is sought to remove the road torque component. In this way, an estimate of the torque sensor can be constructed. The other systems in a vehicle equipped with EPS communicate through a CAN network; hence, signals utilized in other vehicle control systems could be used in this application, assuming fault diagnosis techniques are also applied to those systems as well. This section details the vehicle and tire dynamics necessary to estimate the low frequency, aligning component of road torque.

The equations presented in the subsequent paragraphs are based on lateral vehicle dynamics - namely the bicycle vehicle model and the linear tire model, which have been widely adopted for vehicle dynamics control [20]. In each model, assumptions are made which are valid for most typical driving conditions in order to describe the system with linear equations. However, during more extreme vehicle maneuvering, that is, as the tire slip angle exceeds the maximum tire/road contact grip (see *Figure 2.7*), the system becomes heavily non-linear. Furthermore, the cornering stiffness  $C_\alpha$  is assumed constant; however, it increases with tire pressure. When the car turns, the mass transfer onto the external wheels increases with increased tire pressure; however, variations are less than 10%, so the linear model is still a good approximation. In the following, lateral tire/road forces  $F_y$  are taken to be linear, which is reasonable when lateral acceleration of the vehicle is less than 0.4 g [8].

One of the most significant functions of a tire is to generate lateral forces to control vehicle direction. As the tires deform with slip angles, as shown in *Figure 2.7*, the tires of a vehicle produce lateral forces in proportion to this slip. The slip angle  $\alpha$  represents the angle between the tire's direction of travel and longitudinal axis. As the tire rolls, the tire contact patch with the ground deforms along the direction of travel. It is this deformation and the elasticity of the tire that produces the lateral tire force  $F_y$ .



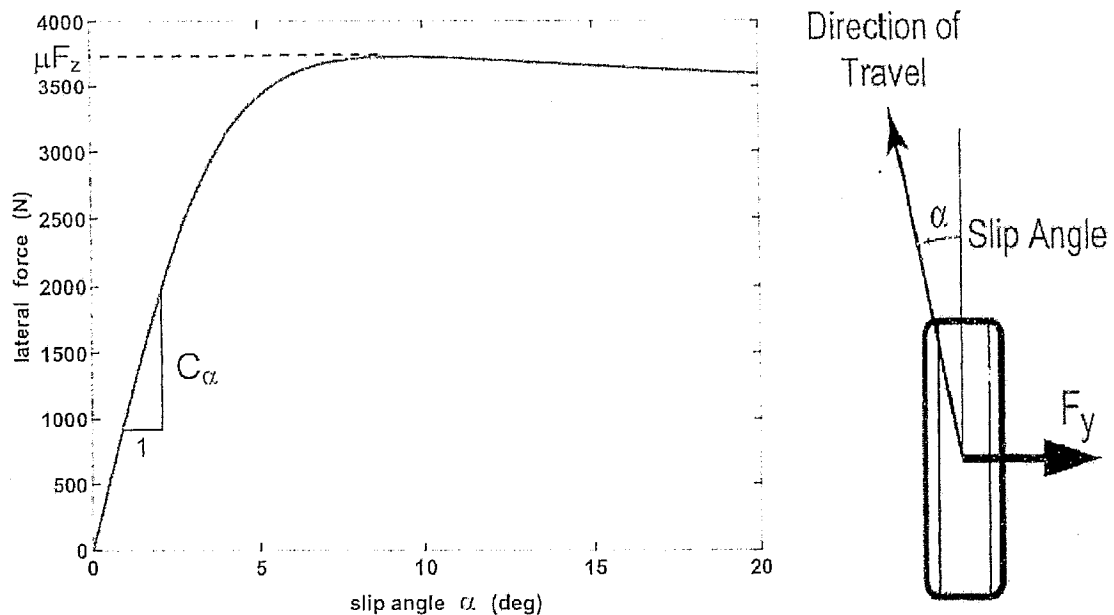


Figure 2.7: Tire Deformation (Causing lateral force) versus slip angle

In Figure 2.7 a typical trend of the lateral force as a function of slip angle is provided, as detailed in [41]. In the linear operating region of the tire curve (small slip angles, which correspond to most driving conditions) the lateral force of the tire can be modeled as:

$$F_y = C_\alpha \alpha \quad (2-1)$$

Conceptually,  $C_\alpha$  is a property of the tire and is mostly independent of the amount of tire grip available, which is described by  $\mu$ , the friction coefficient between the road and tire. This model assumes no significant longitudinal forces and a uniform pressure distribution. Figure 2.7 shows that the lateral force and slip angle are initially linear with cornering stiffness  $C_\alpha$ . If the vehicle is maneuvered very aggressively, however, the lateral force starts to saturate due to limited friction between the tire and road surface. At this point, the vehicle enters a non-linear handling region. When driving, this results in the perception of an impending loss of control over the vehicle. The extreme case: on a completely frictionless surface, you can turn the wheels, but your direction of travel will not change.

Hence, from *equation 2-1*, if the tire slip can be determined, the lateral force, and in turn the torque due to the lateral forces, can be calculated from it. In order to calculate the slip angle, vehicle dynamic equations are employed, which are typically utilized in vehicle stability and other vehicle control systems. The lateral dynamics of a vehicle in the horizontal plane are represented by a bicycle model with states lateral velocity  $V_y$  and yaw rate  $r$ . The underlying assumptions are that the slip angles on the inside and outside wheels are small and identifiable, and the suspension roll has small effect. Additionally, this model assumes negligible lateral weight shift, roll and compliance steer while traveling on a smooth road. Using the model shown in *Fig. 2.8*, the equations of motion for the bicycle model can be written:

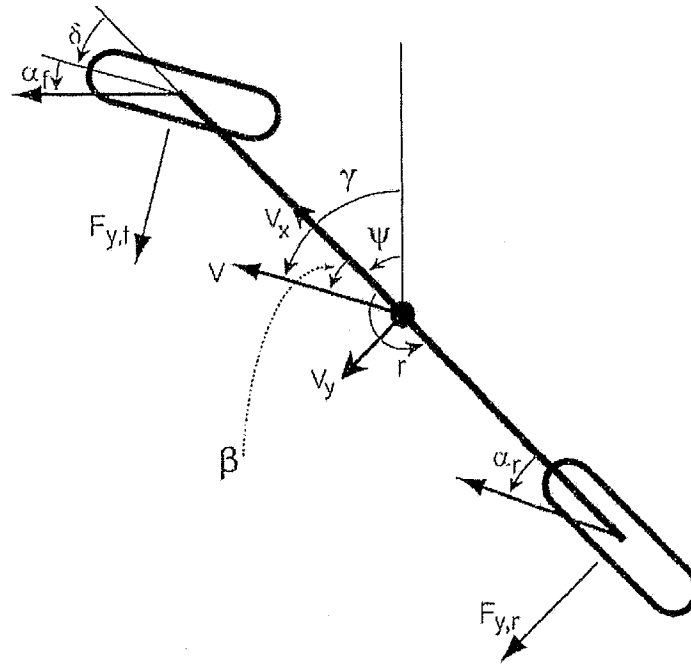


*Figure 2.8: Planar Bicycle Model*

$$ma_y = F_{y,f} \cos \delta + F_{y,r} \quad (2-2)$$

$$I_z r = aF_{y,f} \cos \delta - bF_{y,r} \quad (2-3)$$

Linearized with small slip angles, the front and rear slip angles can be written in terms of  $V_x$ ,  $V_y$ ,  $r$ , and  $\delta$ :

$$\alpha_f \approx \frac{V_y + a_r}{V_x} - \delta \quad (2-4)$$

$$\alpha_r \approx \frac{V_y - br}{V_x} \quad (2-5)$$

If the vehicle's longitudinal speed is considered constant with respect to the lateral dynamics, and the lateral acceleration is sufficiently small that the tire slip / lateral force relation is linear, then *equations 2-2 through 2-5* can be written in state space form. Under these conditions, the lateral vehicle dynamics can be described by a 2<sup>nd</sup> order linear system:

$$\dot{x} = \mathbf{A}x + \mathbf{B}u \quad (2-6)$$

$$\text{where } \mathbf{A} = \begin{bmatrix} \frac{-C_{\alpha,f} - C_{\alpha,r}}{mV_x} & -V_x + \frac{C_{\alpha,r}b - C_{\alpha,f}a}{mV_x} \\ \frac{C_{\alpha,r}b - C_{\alpha,f}a}{I_z V_x} & \frac{-C_{\alpha,f}a^2 - C_{\alpha,r}b^2}{I_z V_x} \end{bmatrix}$$

$$\text{and } \mathbf{B} = \begin{bmatrix} \frac{C_{\alpha,f}}{m} \\ \frac{C_{\alpha,f}a}{I_z} \end{bmatrix} \quad x = \begin{bmatrix} V_y \\ r \end{bmatrix} \quad u = \delta$$

The driver and EPS motor are subject to the effect of these forces through a total moment about the pinion axis. The lateral tire forces are transferred through the tires/tie rods to the rack/pinion connection. This total aligning moment is proportional to the lateral tire force by the distance the force is applied from the steering axis, known as the total trail, as can be seen in *Figure 2.9*. The trail is a function of the mechanical trail  $t_m$  as well as the pneumatic trail  $t_p$ . The pneumatic trail is the distance between the resultant point of

application of lateral force and the center of the tire, whereas the mechanical trail is the distance between the tire center and the steering axis, which is a constant function of steering geometry. Pneumatic trail, however, depends on front slip angle  $\alpha_f$ , and the two tire parameters  $C_{\alpha_f}$  (front cornering stiffness) and  $\mu$  (coefficient of friction between the road and tire surfaces) [22].

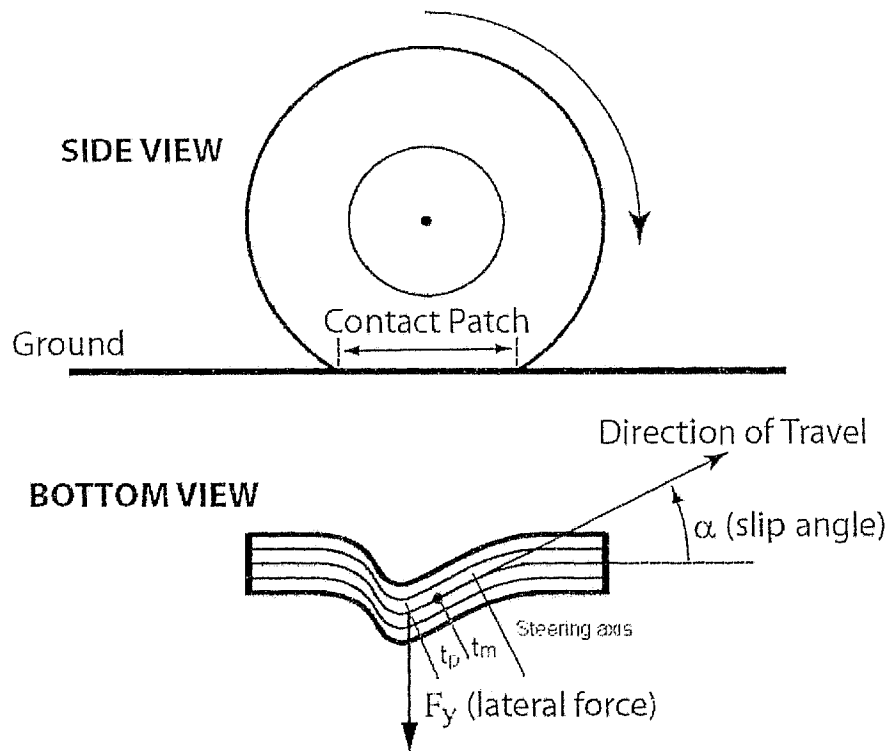


Figure 2.9: Rolling Tire Deformation and Lateral Force

However, for small slip angles (typical driving conditions and linear region of tire model) the pneumatic trail is approximately a constant as well, see [3]. Hence,

$$T_{align} = -(t_p + t_m)F_{y,f} \quad (2-7)$$

This is the torque that tends to turn the wheels back to center position, and is due the interaction between the road and tire surface.

## 2.5 Observer Theory

The Kalman filter, which is an observer designed with optimal criteria, uses knowledge of the process noise covariance  $\mathbf{Q}$ , sensor noise covariance  $\mathbf{R}$ , system and measurement model  $(\mathbf{A}, \mathbf{B}, \mathbf{C})$ , control inputs  $u_k$ , and measured outputs  $y_k$  to reconstruct the states  $x_k$ . It was first formulated in discrete time due to more straight forward mathematics and ease of digital computer implementation, but can be extended to the continuous time case for analysis or problem formulation purposes. It is perhaps the mostly widely used state estimator: it not only works well in practice, but it is theoretically attractive because it can be shown that of all possible filters, it is the one that minimizes the variance of the estimation error. Kalman filters are often implemented in embedded control systems because in order to control a process, accurate estimates of the process variables are needed. The end result of a Kalman filter (filter meaning a data processing algorithm) are a set of equations, which would be updated at every successive time step,  $k$ . The discrete time case for the Kalman filter is described in the following paragraphs; afterwards, the continuous time case for the pole placement technique is presented.

The Kalman filter generates a pre-measurement estimate of the system states based on the measured input and model. A post-update estimate is generated by updating the states based on a number of noisy measurements, which are weighted by a gain matrix  $\mathbf{K}_k$ . The time varying matrix gain  $\mathbf{K}_k$  is obtained by minimizing  $\mathbf{P}_k$  (the variance of the estimation error, the difference between the true and estimated states) throughout time. A derivation of the propagation of  $\mathbf{P}_k$  and the filter equations can be found in [34]. The Kalman filter can be derived and equations arranged in many different ways; the solution presented here is only one of many. Note that since the Kalman filter is a recursive linear estimator, when the states are constant ( $\mathbf{A}=\mathbf{I}, \mathbf{Q}=0$ ) the algorithm reduces to least squares regression. The Kalman filter is a recursive algorithm, so the current estimates are calculated from the previous estimates, as follows. The error covariance  $\mathbf{P}_k$  is minimized throughout time via the discrete time Riccati equation:

$$\mathbf{P}_{k+1} = \mathbf{A}\mathbf{P}_k\mathbf{A}^T + \mathbf{Q} - \mathbf{A}\mathbf{P}_k\mathbf{C}^T\mathbf{R}\mathbf{C}\mathbf{P}_k\mathbf{A}^T \quad (2-8)$$

The time varying matrix filter gain is calculated as:

$$\mathbf{K}_k = \mathbf{A}\mathbf{P}_k\mathbf{C}^T(\mathbf{C}\mathbf{P}_k\mathbf{C}^T + \mathbf{R})^{-1} \quad (2-9)$$

The actual calculation of the states uses the predictor (estimating the next value of the state based on the current states, system model and inputs) and corrector (updating the estimate with measurements) structure:

$$\hat{x}_{k+1} = (\mathbf{A}\hat{x}_k + \mathbf{B}u_k) + \mathbf{K}_k(y_{k+1} - \mathbf{C}\hat{x}_k) \quad (2-10)$$

The amount that the states  $x_{k+1}$  are corrected depends on the relative magnitude of  $\mathbf{Q}$  and  $\mathbf{R}$ . For example, if  $\mathbf{Q}$  is large (we are not very certain about our process model) and  $\mathbf{R}$  small (our measurements are not very noisy), the gain  $\mathbf{K}$  will be large. This results in a greater weight given to the measurements and a filter with a higher bandwidth (that is, the measurements correct the estimated states quicker). Likewise, if the sensors are very noisy ( $\mathbf{R}$  large) but our process model well known ( $\mathbf{Q}$  small), the filter gain will be small. This results in little credibility given to the measurements.

Note that in most linear system cases, the error covariance matrix  $\mathbf{P}_k$  and the optimal filter gain  $\mathbf{K}_k$  quickly reach steady state values; hence, the time varying gain can be replaced by a pre-computed, constant value. This is called a steady state Kalman filter.

Unlike Kalman filters, deterministic or classical observers are typically described in continuous time. They use the same predictor/corrector structure described previously:

$$\dot{\hat{x}} = \mathbf{A}\hat{x} + \mathbf{B}u + \mathbf{L}\mathbf{C}(x - \hat{x}) \quad (2-11)$$

In order for the state estimation error to converge to zero, the error dynamics must be

stable, and the control inputs and sensor outputs must be accurately weighted in the system model, that is  $\hat{\mathbf{B}} = \mathbf{B}$ ,  $\hat{\mathbf{C}} = \mathbf{C}$ . Moreover, in order for the estimation scheme to have little impact on the controller, it is important that the estimation error converges to zero quicker than the states converge to a steady state value in the case of system step response:

$$\dot{e}_x = (\mathbf{A} - \mathbf{LC})e_x, \quad \text{such that} \quad \min \text{time}(e_x \rightarrow 0) \quad (2-12)$$

Furthermore, the poles of the error dynamics must be in the left hand plane for the estimator to be stable. This is normally accomplished by placing the poles of  $\mathbf{A} - \mathbf{LC}$  a magnitude greater than the poles of the system dynamics. In this estimator design, the trade-off between noise sensitivity and process uncertainty (in the Kalman filter, the matrices  $\mathbf{Q}$  and  $\mathbf{R}$ ) is indirect. The faster we make the error dynamics ( $\mathbf{L}$  larger based on larger poles of  $\mathbf{A} - \mathbf{LC}$ ), the more sensitive the filter becomes to sensor noise and errors; relatively, the less sensitive it becomes to process variations.

Note that an observer can be viewed intuitively as a feedback control system designed to drive the residual between the estimated and measured states,  $y - \mathbf{C}\hat{x}$ , to zero.

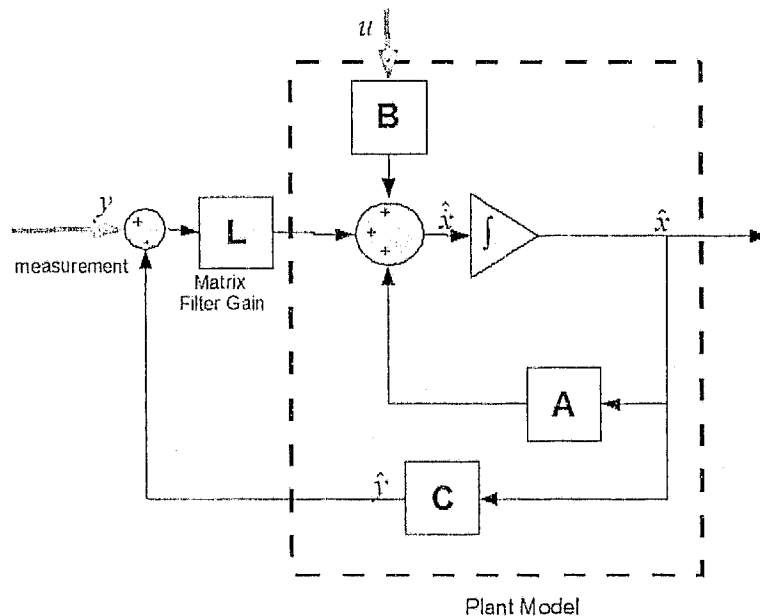


Figure 2.10: Observer viewed as a Feedback system

## CHAPTER 3

### DESIGN AND METHODOLOGY

The problem that will be addressed in this thesis is that of a torque sensor failure; the approach taken to remedy this failure is to estimate the signal based on other relatively more reliable motor signals. This torque sensor estimate can then be used for fault detection by generating a residual signal  $R_{ts}$ , which continuously compares the actual torque sensor output voltage to the estimated signal:

$$R_{ts} = \left| T_{ts} - \hat{T}_{ts} \right| \quad (3-13)$$

A failure in the torque sensor occurs if the residual becomes too large:

$$R_{ts} > K_{thresh} \quad (3-14)$$

Note that the threshold would be determined experimentally from actual vehicle experiments. It should be set high enough as to not produce false faults. Since it is only desired to detect a complete torque sensor failure, and not incipient or drifting soft faults, additional criteria can be introduced to alleviate this problem. For instance, an additional AND criteria to check whether the torque sensor is outputting an invalid, ground, or null voltage could be used.

More importantly, the estimated torque sensor signal can be used to replace the faulty signal as a command to the EPS motor. This is inherently more difficult than simply estimating the signal for fault detection purposes, as the estimated signal is entered as a command to the motor current (torque) control loop. Thus, the estimation dynamics interfere with the motor electric dynamics. The said effects of estimation error in the signal (due to parameter variations, unmodelled dynamics, sensor offsets, etc) are explained and results presented in *Chapter 4*.



### 3.1 Estimating Shaft Torque via Motor Model Based Observer

In order to extract applied torque information from the motor, it is important to understand how the torque sensor operates with respect to the motor shaft. In principle, the torque sensor estimates the driver's instructional torque. This is accomplished by placing a torsion bar between the steering and pinion side shafts; the twist (difference between the angular positions) of the torsion bar is proportional to the driver's torque:

$$T_{ts} = K_s(\theta_p - \theta_{sw}) \quad (3-15)$$

Where  $K_s$  is the spring/stiffness constant of the torsion bar. This equation neglects the dampening effect, which adds a slight lag to torque sensor output. This calculated torsion torque is converted to a voltage signal and input to a conventional EPS motor drive system, shown in *Figure 1.1*. The EPS control model is developed in [5] and shown in *Figure 2.6*, where the torque sensor and DC motor subsystem are highlighted.

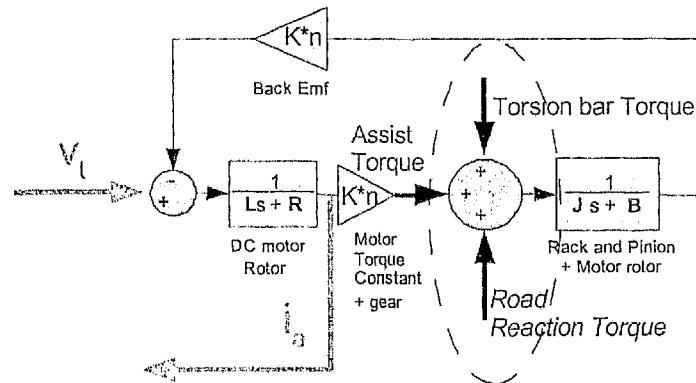


*Figure 3.11: DC Motor Subsystem of an EPS system*

This electrical torque sensor signal is also available through the mechanical torsion torque. The torsion torque and the road reaction torque are reflected onto the motor shaft through the gearbox, as illustrated in *Figure 3.11*. The steering demand torque to the motor drive is normally the torque sensor; the armature current is measured to use as a

feedback signal for this electromagnetic steering assist torque. A command voltage is generated (typically using a PI controller) and is applied to the armature winding. In the faulted case, this command will be based on an estimated torque sensor value. This also effects how the resulting motor dynamics behave, since the estimation scheme participates in the control loop:

$$V_t = (K_p + K_i \int dt)e, \quad \text{where } e = G\hat{T}_{ts} - Ki_a \quad (3-16)$$

A PI controller is chosen because of its inherent strong robustness, ease of implementation and modification, and removal of steady state error between the command and generated motor torque.

Now that the motor usage and how it interacts with the torque sensor is put into perspective, the motor dynamics can be used to gain insight into how the torque sensor signal might be estimated. With only the net applied torque  $T_L$  considered on the motor, the mechanical dynamics on the rotor shaft are modeled using a linear model, which neglects dry and higher order friction:

$$T_m = Ki_a = J_m \frac{d}{dt} \omega_m + B_m \omega_m + T_L \quad (3-17)$$

Ignoring the rack and pinion inertial/viscous friction torque  $T_{rp}$  (which can be calculated separately or incorporated into the motor's inertia and friction) the total load/disturbance torque  $T_L$  is:

$$T_L = \frac{(-T_{ts} + T_{road})}{n} \quad (3-18)$$

By examining *equation 3-17*, if  $\omega_m$  were available in addition to the current measurement  $i_a$ , and the nominal parameters known accurately, the total load torque could be calculated from the mechanical dynamics alone.

However, as measurements of the terminal voltage  $V_t$  (which is actually a time averaged PWM signal; the original command voltage from the output of the controller would be used) and armature current  $i_a$  are available with a standard EPS system, the motor rotor's electrical dynamics could be utilized as well. This is due to the fact the motor's angular velocity is proportional to the back EMF  $V_{emf} = K\omega_m$ , linking the mechanical and electrical dynamics. Neglecting magnetic saturation and the voltage drop across the brush/commutator interface (which is typically small), the motor's electrical dynamics can be written as follows:

$$V_t = R_a i_a + L_a \frac{d}{dt} i_a + K \omega_m \quad (3-19)$$

Using methods detailed in the subsequent paragraphs,  $T_L$  can be obtained from knowledge of  $V_t$ ,  $i_a$  and the motor model. The next section will detail how the low frequency road reaction torque is estimated separately, and the high frequency component filtered out.

Since *equations 3-17 and 3-19* are linked through motor's angular velocity  $\omega_m$  and armature current  $i_a$ , state estimation techniques can be used to estimate the total shaft load or disturbance torque. In principle, an observer (a type of state estimator) uses a copy of the nominal plant and control input ( $V$ ) to produce an estimate of the system states  $x$ , which are corrected by comparing at least one measured output ( $i_a$ ) to its estimated value. This form of estimation is possible if the system is observable, meaning there are sufficient outputs (sensors) and corresponding linear differential equations to solve for the unmeasured states.

Classic observer theory can be applied to a plant well described by linear differential equations with known inputs. In practice, the EPS motor's overall normal behaviour is linear, but is subject to various disturbances (from the road, driver, and vehicle). As well, the motor is also subject to other nonlinear effects: a relatively negligible voltage drop

due to brush/commutator interface, thermal variations (especially in effective resistance  $R_a$ ), dry friction on the motor shaft, and magnetic flux saturation, which results in less torque output per unit current (smaller flux linkage  $K$ ). In this work, the linear model is considered; the feedback mechanism of observers allows parameter variations and some non-linearity to be tolerated. Significant effects such as magnetic flux saturation could be dealt with directly by increasing the steering assist gain when saturation is reached, in order to compensate for the loss of torque per unit current. Moreover, an extended state filter (i.e. the extended Kalman filter) that addresses the non-linear flux  $K$  could possibly be used.

The target is to estimate the torsion bar torque  $T_{ts}$  by estimating the total load on the motor shaft  $T_d$ , an input/disturbance that is neither measurable nor predetermined. Classic observer theory applies to systems with known inputs only: it can be extended by either considering  $T_d$  an unknown input or as a state variable. The later has superior estimation performance [11]. If considered a state variable, some sort of assumption must be made about  $T_d$  in order to describe its dynamics by ODEs. If  $T_d$  varies much more slowly than the other system states, it is possible to assume that  $T_d$  is constant with respect to the motor dynamics.

The equations of the DC motor connected to the EPS system, from which the observer is derived and analyzed, are presented below, using a procedure similar to that found in [36]. The motor is either a fixed field or permanent magnet DC motor (constant flux linkage constant  $K$ ).

Mechanical dynamics at the motor shaft:

$$T_m = Ki_a = J_m \frac{d}{dt} \omega_m + B_m \omega_m + \frac{T_d}{n} + \Delta T_p \quad (3-20)$$

$$\text{where } \Delta T_p = -(\Delta K)i_a + (\Delta J_m) \frac{d}{dt} \omega_m + (\Delta B_m) \omega_m$$

$$\text{and } T_d = -T_{ts} + T_{road} + J_{rp} \frac{d}{dt} \omega_p + B_{rp} \omega_p$$

Electrical dynamics of the motor's rotor armature circuit:

$$V_t = R_a i_a + L_a \frac{d}{dt} i_a + K \omega_m + \Delta V_p \quad (3-21)$$

$$\text{where } \Delta V_p = (\Delta R_a) i_a + (\Delta L_a) \frac{d}{dt} i_a + (\Delta K) \omega_m$$

Here the parameters represent the motor's nominal values that will be used in the observer design. Variation between the current physical parameters and the nominal ones used in the observer (indicated by  $\Delta$ ) are tolerated by correcting the state estimates (which would become incorrect otherwise if only the model was used) with measurement of the motor armature current. Many state estimation techniques employ this predictor/corrector structure.

This predictor/corrector structure of state estimators make them robust, in most cases, in terms of eventually reaching the correct steady state value (assuming no input or output sensor offsets). However, this is not necessarily the case when an estimated disturbance is used in control of the system. A state controller cannot be designed for this faulted torque sensor case as the system in *equation 3-24* is not controllable. However, the torsion bar component of  $T_d$  can be fed forward as the input to the motor torque loop. In this case, the estimation error interferes with the motor operation per *equation 3-16*. Hence, the effects of the parameter variations (which cause estimation error) are considered separately, which are represented by  $\Delta$ . These parametric variations cause torque and voltage disturbances labeled  $\Delta T_p$  and  $\Delta V_p$ , respectively. Their effects on the FTC scheme developed in this chapter are explored in Chapter 4.

The overall motor dynamics in an EPS system, including modeling uncertainty, is described in *equations 3-20, 3-21*. The sign of  $T_{road}$  is chosen to represent the fact the road torque opposes the motion of the applied torques,  $T_m = K i_a$  and  $T_{ts}$ . To retain model

linearity  $T_d$  is considered a state variable; however, in order to describe its dynamics by ODEs required for the state space description, some sort of assumption must be made about its behaviour. If  $T_d$  varies much more slowly than the other system states, it is possible to assume  $T_d$  is a state variable with 0 time rate:

$$\frac{d}{dt}T_d = 0 \quad (3-22)$$

in other words, it assumes the disturbance is varying slowly and independent of the motor dynamics. In addition, the rack and pinion inertia  $J_{rp}$  and viscous friction  $B_{rp}$  torques are considered part of the load torque  $T_d$  such that it is more constant. In this way, the previous assumption is more valid.

This description of a disturbance as an independent, slow varying state variable is called state augmentation [37]. This makes the resulting observer a very powerful tool: not only can it estimate the system's states, it can also estimate the augmented disturbances as well. This assumption of the total load torque on the EPS motor being of lower frequency than the motor subsystem states is realistic. This is because the driver input is typically under 5 Hz and main road wheel dynamics under 10 Hz [8]. These are much slower than a typical servo motor's electrical (torque) response time, governed by the electric time constant  $R_a/L_a$ . A typical motor used for torque control would have an electric time constant less than 0.01 s (100 Hz). Besides, as reported in literature [3,38], this disturbance formulation method holds up for disturbances of much higher frequencies, closer to the frequency of the system's state variables.

An observer can be designed based on the previous motor equations and assumption about the disturbance torque. The motor shaft velocity  $\omega_m$  is not measured in this scheme; although Hall Effect sensors (used in brushless DC motor drives) can be used to obtain a low resolution sample of  $\omega_m$ , it is not sufficient for calculation of the inertial torque in the motor model. Thus, taking into account only the armature current is measured in the EPS DC motor drive, *equations 3-20,3-21, and 3-22* can be written in

state space form, as required to synthesize the observer. In order to more clearly quantify the error dynamics, it is assumed that  $\Delta V_p = \Delta T_p = 0$ , e.g. the actual motor parameters and observer nominal parameters are equal.

$$\dot{x} = \mathbf{A}x + \mathbf{B}u \quad (3-23)$$

$$y = \mathbf{C}x \quad (3-24)$$

$$\text{where } \mathbf{A} = \begin{bmatrix} \frac{-R_a}{L_a} & \frac{-K}{L_a} & 0 \\ \frac{K}{J_m} & \frac{-B_m}{J_m} & \frac{-1}{J_m} \\ 0 & 0 & 0 \end{bmatrix} \quad \mathbf{B} = \begin{bmatrix} \frac{1}{L_a} \\ 0 \\ 0 \end{bmatrix} \quad x = \begin{bmatrix} i_a \\ \omega_m \\ \frac{T_d}{n} \end{bmatrix}$$

and  $\mathbf{C} = [1 \ 0 \ 0] \quad y = i_a \quad u = V_t$

The system  $(\mathbf{A}, \mathbf{B})$  is not controllable, as we cannot effect the load/disturbance torque with the motor voltage input  $V_t$ . However, since the pair  $(\mathbf{A}, \mathbf{C})$  is observable, meaning we can determine the states given measurement of the current, the motor states can be estimated by the predictor/corrector structure:

$$\hat{\dot{x}} = \mathbf{A}\hat{x} + \mathbf{B}u + \mathbf{L}\mathbf{C}(x - \hat{x}) \quad (3-25)$$

With this structure, the corrective term is constructed by comparing estimated states with sensor output measurements, multiplied by a designed matrix gain  $\mathbf{L}$ . Some sort of criteria is used to determine suitable values for  $\mathbf{L}$ ; classic observers and Kalman filters are two such examples. This correction term, the 3<sup>rd</sup> in *equation 3-25*, is used as feedback to drive the estimation error (which is caused by parameter mismatch, unmodelled dynamics, noise, etc) to zero. If filter gain elements are denoted  $L_1, L_2, L_3$ , then the equation describing how the disturbance torque is calculated in the observer is given by integrating the 3<sup>rd</sup> row in *equation 3-25*:

$$\frac{T_d}{n} = L_3 \int (i_a - \hat{i}_a) dt \quad (3-26)$$

This resulting equation is intuitive: neglecting any mismatch between the model and plant, then the error between the predicted value  $\hat{i}_a$  and the measurement  $i_a$  is due to the disturbance  $T_d$  and signal noise.

In this work, the observer filter gain  $\mathbf{L}$  is designed via pole placement such that the error dynamics (*equation 3-25–equation 3-23*)

$$\dot{e}_x = (\mathbf{A} - \mathbf{LC})e_x \quad (3-27)$$

tend to zero faster than the fastest motor dynamics (the rate of change of motor current). Relatively, just as in feedback control systems, the higher the observer gains, the faster the estimated states will converge to their actual values. The filter gains can be designed for faster convergence by placing the poles of  $(\mathbf{A} - \mathbf{LC})$  farther from the  $j\omega$  axis and greater than the poles/eigenvalues of the system dynamics. The higher the filter gain, the more emphasis is put on the output sensors, and less on the value predicted by the model. This decreases sensitivity to modeling errors. Practically, however, the observer gain  $\mathbf{L}$  cannot be made arbitrarily high, as this will increase the observer's sensitivity to noise. Although the output current sensor has high bandwidth and accuracy, offset occurs due to variations in sense resistance; moreover, it has moderate electrical noise levels.

The state error dynamics  $e_x$  are governed by the poles/eigenvalues ( $\lambda$ ) of  $(\mathbf{A} - \mathbf{LC})$ ; similarly, the motor electrical dynamics are governed by the electric frequency  $f_e$ . Hence, the filter gain  $\mathbf{L}$  is designed by placing the poles of  $(\mathbf{A} - \mathbf{LC})$  greater than a factor of three times  $-f_e$ , as in *equation 3-28*. The parameter  $\epsilon$  is chosen a small value (i.e.  $1/100 f_e$ ) for pole placement routines.



$$\lambda(\mathbf{A} - \mathbf{LC}) = -3 \begin{bmatrix} f_e \\ (1 + \varepsilon)f_e \\ (1 + 2\varepsilon)f_e \end{bmatrix}, \quad \text{where } f_e = \frac{R_a}{L_a} \quad (3-28)$$

This is done such that  $e_x$  converges to zero three times faster than the motor current  $i_a$  reaches a steady state value (in the case of a system step response). This design of  $\mathbf{L}$  is chosen because in this setup, there is assumed to be little biased error in the current measurement relative to the DC motor model, which is relatively rough. Hence, the estimation gives significant weight to the current sensor. As well, the pole placement technique provides a good trade-off between noise sensitivity and fast convergence of the estimation error.

To obtain optimal performance (minimizing the average estimation error) in a Gaussian noise (zero mean) environment, a Kalman ( $H_2$ ) filter could be used to design  $\mathbf{L}$ . If biased measurements (perhaps due to current sensor resistor change) and inaccurate modeling were of significant concern,  $H_\infty$  filters could be used as they perform better in face of biased noise (sensor offsets and significant parameter variations). This is because  $H_\infty$  filters minimize the worst case estimation error. Alternately, as in [39], a mixed  $H_2/H_\infty$  filter could be utilized by basing the design criteria on the relative amount of assumed worst case sensor offsets and parameter variations ( $H_\infty$  condition) to the relative amount of optimality ( $H_2$  condition).

With the Kalman filter technique, the following parameters must be chosen to design the filter gain  $\mathbf{L}$ :  $\tau_d$ , which is the parameter that represents the typical rate of change of the disturbance torque,  $\mathbf{Q}$ , the covariance of  $\omega_{process}$  (the plant uncertainty), and  $\mathbf{R}$ , the covariance of  $\omega_{sensor}$  (the sensor noise). Typically, it is possible to measure the standard deviation  $\sigma$  in the sensor's voltage output in order to calculate the variance of the sensor noise. In this way, one can obtain a reasonable value for  $\mathbf{R} = \sigma^2$  (for a single sensor). Selecting the process noise variance  $\mathbf{Q}$  can be more difficult as it depends on how much we trust the system model compared to the measurements. The motor subsystem can be

modeled in the following way in order to design the Kalman filter gains.

$$\dot{x} = \mathbf{A}x + \mathbf{B}u + \omega_{process} \quad (3-29)$$

$$y = \mathbf{C}x + \omega_{sensor} \quad (3-30)$$

$$\text{where } \mathbf{A} = \begin{bmatrix} \frac{-R_a}{L_a} & \frac{-K}{L_a} & 0 \\ \frac{K}{J_m} & \frac{-B_m}{J_m} & \frac{-1}{J_m} \\ 0 & 0 & \tau_d \end{bmatrix} \quad \mathbf{B} = \begin{bmatrix} \frac{1}{L_a} \\ 0 \\ 0 \end{bmatrix} \quad x = \begin{bmatrix} i_a \\ \omega_m \\ \frac{T_d}{n} \end{bmatrix}$$

and  $\mathbf{C} = [1 \ 0 \ 0] \quad y = i_a \quad u = V_t$

In general, this procedure to estimate an unknown disturbance input with the Kalman filter is called a Kalman filter with colored noise [34]. The unknown input can be thought of as a component of the process noise that is non-zero mean; that is, this component of the process noise has substantial low frequency content (it is biased). This gives the component a colored, non white, spectrum.

To determine the steady state Kalman gain (which is only possible for systems with a linear model), we can assume the projected error covariance's rate of change is zero after it converges:

$$\frac{d}{dt} \mathbf{P} = 0 \quad (3-31)$$

The resulting continuous time Riccati differential equations, shown below, are typically solved by decoupling single equations into multiple equations.

The error covariance's steady state value is calculated from the continuous time Riccati equation, which minimizes  $\mathbf{P}$  throughout time:

$$0 = \dot{\mathbf{P}} = -\mathbf{P}\mathbf{C}^T\mathbf{R}\mathbf{C}\mathbf{P} + \mathbf{A}\mathbf{P} + \mathbf{P}\mathbf{A}^T + \mathbf{Q} \quad (3-32)$$

The time-invariant filter gain is calculated using  $\mathbf{P}$ :

$$\mathbf{L} = \mathbf{P}\mathbf{C}^T\mathbf{R}^{-1} \quad (3-33)$$

The actual filter uses the previously discussed predictor/corrector structure:

$$\hat{\mathbf{x}} = \mathbf{A}\hat{\mathbf{x}} + \mathbf{B}u + \mathbf{L}(y - \mathbf{C}\hat{\mathbf{x}}) \quad (3-34)$$

The noise matrices ( $\mathbf{Q}, \mathbf{R}$ ) are calculated as:

$$\mathbf{Q} = \begin{bmatrix} \sigma_{electrical}^2 & 0 & 0 \\ 0 & \sigma_{mechanical}^2 & 0 \\ 0 & 0 & \sigma_{disturbance}^2 \end{bmatrix}, \mathbf{R} = \sigma_{current\ sensor}^2 \quad (3-35)$$

$\sigma_{electrical}^2$ , for example, represents the variance between the estimated and actual electrical dynamics. The motor model is subject to a significant amount of uncertainty: uncertainty in the nominal parameter measurements ( $\pm 10\%$  or more) and unmodelled dynamics (for example, brush/commutator and thermal effects). The current sensor, on the other hand, is mostly effected by electrical noise (due to EMI, power supply, PWM), as well as uncertainty in the sense resistor value. Since the motor's parameter's are subject to more uncertainty than the current measurement, the sensor output is trusted more than the process model. This is indicated by choosing  $\mathbf{Q} > \mathbf{R}$ . For example, the following values can be chosen:

$$\mathbf{Q} = (4\mathbf{R})\mathbf{I} \quad , \quad \mathbf{R} = \sigma_{current\ sensor}^2 \quad (3-36)$$

where  $\mathbf{I}$  is a 3x3 identity matrix. Solving the Riccati equation in *equation 3-32* for  $\mathbf{P}$ , then solving for the Kalman gain  $\mathbf{L}$  in *equation 3-33* will result in a filter that attempts to

minimize the average error. However, as the Kalman filter has the same predictor/corrector structure as the Luenberger observer (*equation 3-28*), it exhibits similar errors when the estimated torque is used as a control input to the motor drive.

Either of the previously described methods, when used for fault detection only, are robust to steady state estimation error caused by bounded plant variations. However, when the torque sensor estimate is used as the control input, it interferes with the overall motor system dynamics. This is because the observer itself forms a dynamic feedback system. This results in steady state estimation error despite the observer corrective feedback if there are unmodelled disturbance inputs ( $\Delta V_p$  and  $\Delta T_p$ , caused by parameter variations). However, this error is bounded as long as the parameters used for the observer are close to their real motor counterparts. Even if the motor parameters vary significantly, this will only result in less steering assist available to the driver. These results will be presented in Chapter 4.

### 3.2 Estimating Road Torque from Vehicle and Tire Dynamics

As previously discussed, the aligning component of the road torque can be determined from measurable vehicle parameters and tire slip angle. The tire slip angle is calculated from vehicle velocities and yaw rates, as in *equation 3-50*; in the linear operating region for which these equations are valid, the lateral vehicle dynamics can be described by *equation 3-52*. These signals are available in inertial navigation systems (INS), which are commonly used for vehicle stability systems.

Vehicle Stability Control (VSC) systems control the yaw rate of the vehicle to prevent understeer and oversteer. The actuation to accomplish this is an Anti-Lock Braking System (ABS), which modulates the brake pressure in order to control the friction between the tire and road. Moreover, VSC and similar vehicle control systems (such as roll stability) require an INS or similar set of sensors to measure/estimate the vehicle dynamics. By 2010, the US and Canadian governments are requiring ABS and VSC in all new vehicles.

In an INS, accelerometer and gyroscope measurements are integrated to obtain vehicle lateral  $V_x$  and longitudinal  $V_y$  velocities and yaw rate  $r$ . These signals, combined with the steering angle  $\delta$  (provided by the motor shaft position signal through gear  $n_g$  and steering  $n_s$  ratios) are used to estimate the aligning moment:

$$T_{align} = -t_o \left[ \frac{V_y + ar}{V_x} - \delta \right] \quad (3-37)$$

$$\text{where } t_o = (t_p + t_m)C_\alpha, \quad \delta = \frac{\theta_m}{n_s n_g}$$

$$\begin{aligned}
 V_y &= V_{y(o)} + \int a_y dt \\
 V_x &= V_{x(o)} + \int a_x dt \\
 r &= r_{(o)} + \int \dot{r} dt
 \end{aligned}$$

Integrating the gyroscope and accelerometer measurements  $\dot{r}$ ,  $a_y$ , and  $a_x$  results in drifting yaw rates and velocities; this can be avoided by an expensive mounting configuration and very high speed, precise rotational equipment [20]. This is typically only used in applications that can justify the cost, i.e. aviation. However, if a two antenna GPS system is integrated into the vehicle, absolute measurements of the slippage angle are available, which can be used to calculate the lateral velocity and yaw rate. The vehicle slippage angle  $\beta$  (refer to *Figure 2.8*) can be defined by:

$$\beta = \tan^{-1} \left( \frac{V_y}{V_x} \right) \approx \frac{V_y}{V_x} \quad (3-38)$$

The slippage angle can also be defined as the difference between the vehicle yaw angle  $\psi$  and direction of velocity  $\gamma$ , see *Figure 2.8*, both of which are measured in a two antenna GPS.

$$\beta = \gamma - \psi \quad (3-39)$$

The vehicle yaw rate is obtained directly from differentiation of the GPS yaw angle  $\psi$ , and the vehicle velocities can be calculated from the absolute velocity and the slip side angle:

$$V_x = |V| \cos \beta \quad (3-40)$$

$$V_y = |V| \sin \beta \quad (3-41)$$

$$r = \frac{d}{dt} \psi \quad (3-42)$$

The GPS signals from *equations 3-40 to 3-42* could be used exclusively to calculate the tire slip. However, the refresh rate of the GPS signals (typically 5 Hz) is insufficient for vehicle stability control or this EPS application. Instead, they can be used to periodically update the values of the faster INS signals, in order to correct for the integration drift. This can be accomplished using Kalman filter techniques, which effectively combine the sensors (accelerometer, gyroscope, and GPS) to obtain more accurate vehicle state estimates, see [22]; furthermore, this model can be extended to consider road grade and other factors. When the GPS signal is not available or is not installed, other techniques can be used to reduce the integration drift, such as periodically zeroing and recalibrating during straight-ahead driving.

In this work, the aligning component is considered the major contributor to the low frequency road torque. Other torques are present on the pinion shaft, as presented in [7], and summarized in the following table:

*Table 3.I: Frequency of Road Information*

Torques on Rack/Pinion <i>due to road reaction and /vehicle vibrations</i>	Frequency
Reaction forces related to vehicle motion	0 to 10 Hz
Resonant frequency of EPS mechanical components	10 -- 13 Hz
Resonant frequency of suspension	13 to 17 Hz
Shimmy	15 to 25 Hz

For instance, [22] models a jacking torque component of the road torque, which is attributed to vertical vibration caused by rough roads and terrain. This jacking torque and other higher frequency road torques are considered a random signal that must be filtered out rather than estimated. This is possible since this information occurs at higher frequencies than the aligning torque and driver input related to vehicle motion. Hence, the road torque is estimated as:

$$\hat{T}_{road} = T_{road(LF)} \approx T_{align} = -C_{\alpha,f} (t_p + t_m) \alpha_f \quad (3-43)$$

$C_{\alpha}$ ,  $t_p$  and  $t_m$  are constants in the linear stable handling region of the vehicle for which these equations are valid. The tire slip  $\alpha_f$  is calculated from INS signals as per *equation 3-37*. The rough road torque is filtered out of the total estimate  $T_d$  by means of a low pass filter with a cutoff frequency of 10 Hz. This preserves the driver's feel and road feedback information but removes the higher frequency component due to the rough road surface.



### 3.3 FTC of EPS by combining previous methods

All of the previously discussed techniques were ultimately used to obtain an estimate of the torsion torque that is applied on the motor shaft; in this way, when the torque sensor fails it can be used as the input to the EPS motor drive. This adds a redundant backup system to the torque sensor, enhancing the reliability of the EPS system. An overall structure of this FTC is shown in *Figure 3.12*. This control scheme replaces the existing torque sensor based control, per *Figure 1.1*, upon a fault being detected. A fault occurs when the torque residual  $R_{ts}$ , the difference between the estimated and actual signal, exceeds an experimentally determined threshold.

A torque sensor measures the torsion torque from the difference between two measured angles and knowledge of the stiffness of the torsion bar. In the FTC case, the torsion torque is estimated by it's reflection onto the EPS motor shaft and knowledge of the road reaction torque. This estimated torsion torque is used to reconstruct the torque sensor signal:

$$\hat{T}_{ts} = -h_{LPF}(\hat{T}_d - \hat{T}_{road} - \hat{T}_{rp}) \quad (3-44)$$

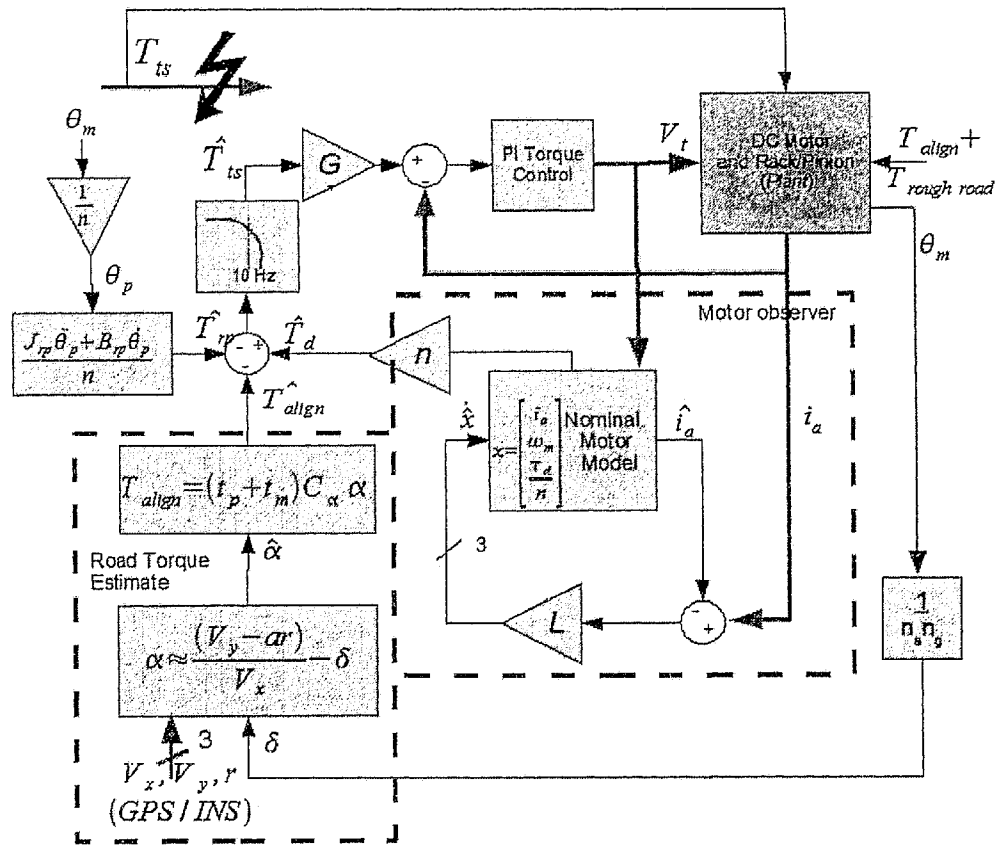


Figure 3.12: EPS Torque Sensor FTC Scheme

The estimation scheme operates in the following manner: the motor model based observer delivers the net disturbance torque  $T_d$  applied to the motor shaft. The road torque is estimated as a linear function of tire slip, which is estimated from navigational signals provided by an INS/GPS. The road torque  $T_{road(LF)}$  is estimated from its predominant low frequency aligning component  $T_{align}$  and is subtracted from the total  $T_d$ . The higher frequency rough road torque and noise in the estimation schemes are filtered out with a low pass filter  $h_{LPF}$ . Furthermore, the inertial and viscous torque due to the rack and pinion connection  $T_{rp}$  is also subtracted out.

In the following Chapter, a hardware-in-the-loop real-time simulation is detailed that is used to validate and test the fault tolerant control scheme and compare it to the conventional torque sensor based control scheme. The test environment is a mix of software (for the vehicle dynamics) and hardware (DC motor and drivers).

## CHAPTER 4

### HIL SIMULATION SETUP AND ANALYSIS

The most reliable and accurate validation of any control design is performed on a full-scale real test; however, such a test can be impractical because of physical limitations, cost considerations, etc. An alternate approach is a HIL simulation platform which imitates the real test locally for the part to be tested and enjoys all of the benefits of numeric simulation for the remainder of the system. It is often used to test a hardware component before the entire system is complete.

In the case of an EPS HIL simulation there is significant environmental impact from the road/tire interaction through the steering linkage. In this case dynamometers can be used to simulate a load on any component such as the EPS motor. Dynamometers are also used as both loads and measurements devices in the testing of other automotive components, such as brakes and engines since it significantly reduces cost and increases repeatability versus testing in-vehicle [45]. Moreover, a HIL simulation can be critical in the development of control systems where the environment is difficult or impossible to control, as in wind turbine electrical generation systems [46]. In [47], HIL simulation of a diesel engine and comparison to in-vehicle data are presented. In this case the remainder of the power-train and vehicle dynamics are simulated in software in order to isolate and study the effects of the various faults that occur in the engine itself.

More realistic simulation such as HIL is especially important for model based control designs, such as those that use observers, state feedback and/or adaptive control. As opposed to classic single loop feedback controllers such as PID, these controllers are often more sensitive to modeling errors which a software simulation cannot fully capture.

### 4.1 Overall Topology

In order to realistically validate the ideas presented in this work, a HIL platform is constructed with an Opal RT™ real-time simulator, see *Figure 4.13*. This platform implements MatLab™ Simulink™ blocks into C code to run in real time. The platform is equipped with a PC with a real-time O/S, QNX, and I/O cards to interact with the physical hardware. The most significant hardware in the work is the EPS motor subsystem of the EPS. One DC motor drive acts as the EPS subsystem. Another coupled motor is used as a dynamometer, which applies the calculated vehicle dynamic

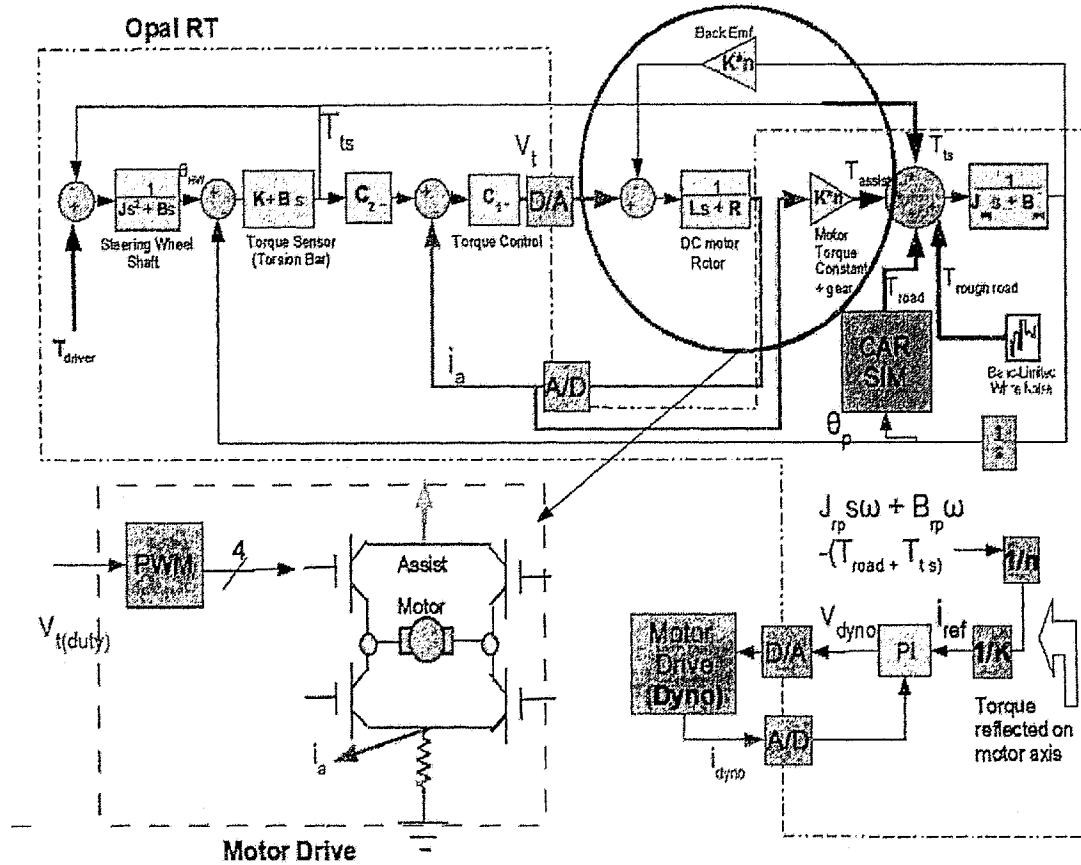


Figure 4.13: EPS HIL Simulation Model Based Description

torques onto the EPS motor. The torsion bar torque  $T_{ts}$ , rack and pinion inertia/viscous friction  $T_{rp}$ , and road torque dynamics  $T_{road}$  are simulated in real time. This is accomplished by both running the models in software and applying the calculated torques

onto the EPS motor shaft via the dynamometer, to compensate for the load that is not physically connected.

Both the EPS and dynamometer motors are operated with a fixed field; in this way, the torque is directly proportional to current. The dynamometer rotor is coupled to the EPS motor rotor with a rigid connection. This allows the dynamometer's torque to follow the simulated load dynamics quickly and accurately, applying them directly to the EPS motor shaft. Since these torques are calculated on the steering/pinion shaft, to reflect onto the motor axis, they are divided by the EPS motor gearbox ratio  $n$ , and the motor's current to torque relationship  $K$  in order to generate a corresponding current demand to the PI controller.

The EPS and dynamometer motor currents are measured via the voltage across a sense resistor, placed in series with the motor armature windings, and is sampled at a rate of 1000 Hz. As per *Figure 4.17*, this current signal is used as a feedback signal for torque control, as a corrective signal to the observer, as well converted to a torque value and applied on the rack and pinion simulated dynamics.

CarSim™ is utilized to provide a realistic road torque signal to input to both the simulated vehicle/torque sensor dynamics, and to the EPS motor via the dynamometer. To simulate typical road conditions, a moderate sized sedan under a flat road surface is considered for the results in this thesis. CarSim™ uses experimentally measured steering torque versus steering position data, as well as higher order vehicle models, to calculate the aligning road torque. The simulated pinion angle (which is equivalent to the steering angle of a manual power steering system) is input to the CarSim™ Simulink Block. CarSim™ is configured to accept a steering angle input and output the road reaction torque (labelled steering torque, as they are equal but opposite forces in a manual steering system). This road torque accounts primarily for the low frequency, aligning component only. The high frequency component is due to rough roads, bumps, vibration from the vehicle, etc. To account for the randomness of the rough road torque, this high frequency component is generated from a band-limited random white noise signal.

Besides generating the nominal road torque, CarSim<sup>TM</sup> is used in the validation of the FTC scheme. It provides the yaw rate, lateral and longitudinal velocities of the vehicle being simulated, which are used in the road torque estimation.

## 4.2 Drive Topology for EPS Motor and Dynamometer

On the hardware side, the motor armature terminal voltage  $V_t$ , the control input to the system, is generated as follows. The output calculated by the  $PI$  controller  $C_I$  is converted to a duty ratio (a fraction of the supply voltage). This is converted to a time averaged PWM signal, which drives either leg of an H-Bridge configuration of power transistors that switch current in the motor rotor armature circuit (see *Figure 4.17*). The frequency of the voltage pulse width modulation  $f_{PWM}$  is chosen to avoid excessive current spikes that would occur if the PWM frequency was too low. The higher the frequency of switching, the higher the transistor power losses; however, too low of a PWM frequency causes significant non-linearity in the motor electrical dynamics and thus drastically effects the accuracy of the linear observer outputs. Furthermore, too low of  $f_{PWM}$  effects the smoothness of the EPS motor torque. These conditions can be avoided by choosing:

$$f_{PWM} > 10 f_{electric} = 10 \frac{R_a}{L_a} \quad (4-45)$$

This ensures that the pulse width modulation produces a smooth current waveform.

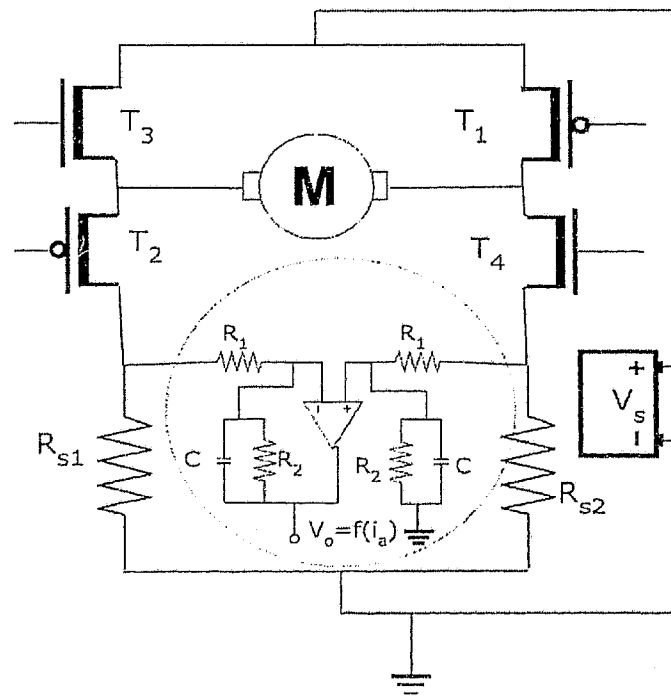


Figure 4.14: Alternate Motor Drive Topology

A motor driver is used that has both PWM signal generation and H-bridge functions integrated onto a single board, which significantly reduces associated wiring. If a microcontroller were used as the controller instead of the simulation platform, it could generate the PWM signal without additional circuitry. Although the Opal RT™ platform can generate PWM signals, it uses a model calculation step and I/O refresh time of 1 ms, which is too slow to provide a smooth current waveform.

Precise bi-directional torque control requires an accurate way to measure the motor's current magnitude and direction. For robust torque control for both the EPS motor and load dynamometer an accurate measurement of the motor current is needed, one that is accurate even around zero current. The current demand in the motor can change direction quickly (limited by the inductance of the motor windings) as it follows the driver's instructional torque input. Hence, the current needs to be measured even when it is switching direction in the armature winding, so the simple one sense resistor scheme of *Figure 4.13* is insufficient. However, it can still be used if measures are taken to correctly identify the current's direction in the control logic.

A configuration using two sense resistors and a high common mode rejection difference amplifier (circled) can be utilized as well, see *Figure 4.14*. In this configuration the power signal (current through the motor armature) is mostly isolated from the sensor signal (the voltage output of the difference amplifier) due to the properties of the operational amplifier. The gains  $R_2/R_1$  can be set to amplify the voltage, in order to utilize the full-scale range of the A/D card. This is especially important if a small sense resistor is used. In order to further improve the current signal Hall Effect or LEM sensors could be utilized instead of resistors; however, in this simulation the lowest cost solution is preferred, as it more accurately reflects a production EPS system.

In this H-Bridge configuration, either  $T_1/T_2$  or  $T_3/T_4$  are switched. Around zero current,  $T_1/T_2$  are switched at the lowest possible duty ratio. This avoids non-linearity caused if the motor was shorted ( $T_2$  and  $T_4$  switched) when no voltage was applied. Due to the inductance of the motor, voltage spikes occur when the motor terminal voltage polarity is



changed; the capacitors are chosen to reduce this effect.

### 4.3 Controller and Simulation Specifics

The motor driver and sense resistor interface with the simulation platform via a data acquisition and output board which are all tied to a common ground to avoid DC offsets between different measurements. These boards use digital-analog and analog-digital converters with 12-bit resolution. The overall platform works with a sampling rate and model calculation step of 1000 Hz / 0.001 sec which is sufficient to calculate the dynamics of the simulated EPS system, observer and controller.

The “torque balance” block *Figure 4.15*, used in *Figure 4.17*, represents the total inertia/dampening effects of the rack and pinion reflected onto the motor shaft axis. This simulates the heavier load on the motor that is not mounted on the motor shaft. In this way, the pinion shaft attached to the motor through the gear reduction is simulated. As well, the simulated rack and pinion shaft receives all the applied torques: torsion bar, road torque, and motor torque (via measurement of the motor current  $i_a$ ).

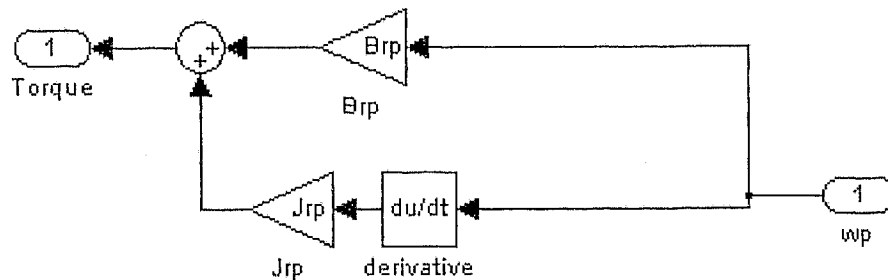


*Figure 4.15: External Torque Balance Block*

The PI controller block of *Figure 4.16* includes logic to avoid integrator windup. This is accomplished by limiting the output of the integrator term and ensuring if the demand is 0, the command voltage to the motor is also 0. If a 1 sense – resistor configuration is used, the relative direction of current is determined by the sign of the current (torque) demand. This works as long as  $T_1/T_2$  are shutoff as soon as  $T_3/T_4$  are turned on. The

two sense resistor configuration of *Figure 4.14* provides a more reliable signal around zero current.

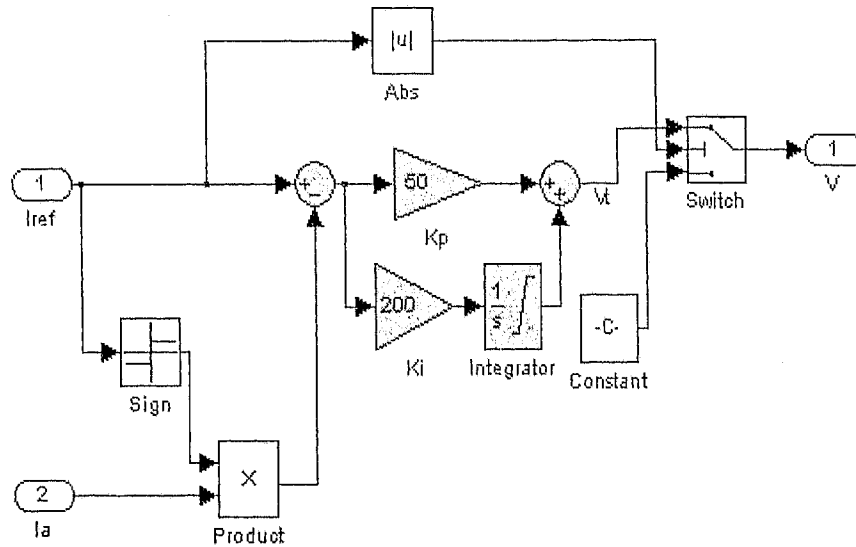


*Figure 4.16: PI Control Logic*

Although the motor and vehicle models utilized in this paper are linear, it is often necessary to compensate for a significant non-linearity in the system. In many control system models the dry Coulomb friction is neglected, because in many systems it is much smaller than the inertial and viscous friction torque components. However, in the HIL simulation with the motor set chosen, this was not the case observed in experimentation. Furthermore, some steering system models include the dry friction component [3]. In the DC motor this friction is mainly due to bearings and brush/commutator interface. In a motor actually connected to an EPS assembly, it would also include the equivalent dry friction of the rack and pinion connection.

For the purposes of keeping the DC motor subsystem model linear, the dry friction  $T_f$  is considered another component of the total disturbance torque  $T_d$ . Hence, the estimated torque sensor signal is calculated as:

$$\hat{T}_{is} = -h_{LFF}(\hat{T}_d - \hat{T}_{road} - \hat{T}_{rp} - \hat{T}_f) \quad (4-46)$$

The static friction torque ( $\omega_m=0$ ), which is the torque the motor must develop to initially starting rotating the shaft, is greater than the dynamic friction torque  $\tau_{fd}$ . Both are constants for constant coefficients of friction. In this simulation, the static friction is ignored (since it is relatively momentary) and the dynamic dry friction is considered. If  $\omega_m$  is not available for measure, the direction of the friction force is opposing the applied force (indicated by the sign of  $V_t$ , neglecting the inductance of the motor). Therefore, the friction torque can be estimated as:

$$\hat{T}_f = -K_f \operatorname{sgn}(\omega_m) \approx K_f \operatorname{sgn}(V_t) \quad (4-47)$$

### 4.4 FTC implementation

The fault tolerant scheme of *Figure 3.12* is implemented on the HIL setup in *Figure 4.13*. The observer and road torque estimation algorithms are implemented in Opal RT™ in parallel with the remaining EPS model with the motor drive in-the-loop. A detailed software and hardware configuration is shown below. *Figure 4.18* shows the overall connectivity of the same setup.

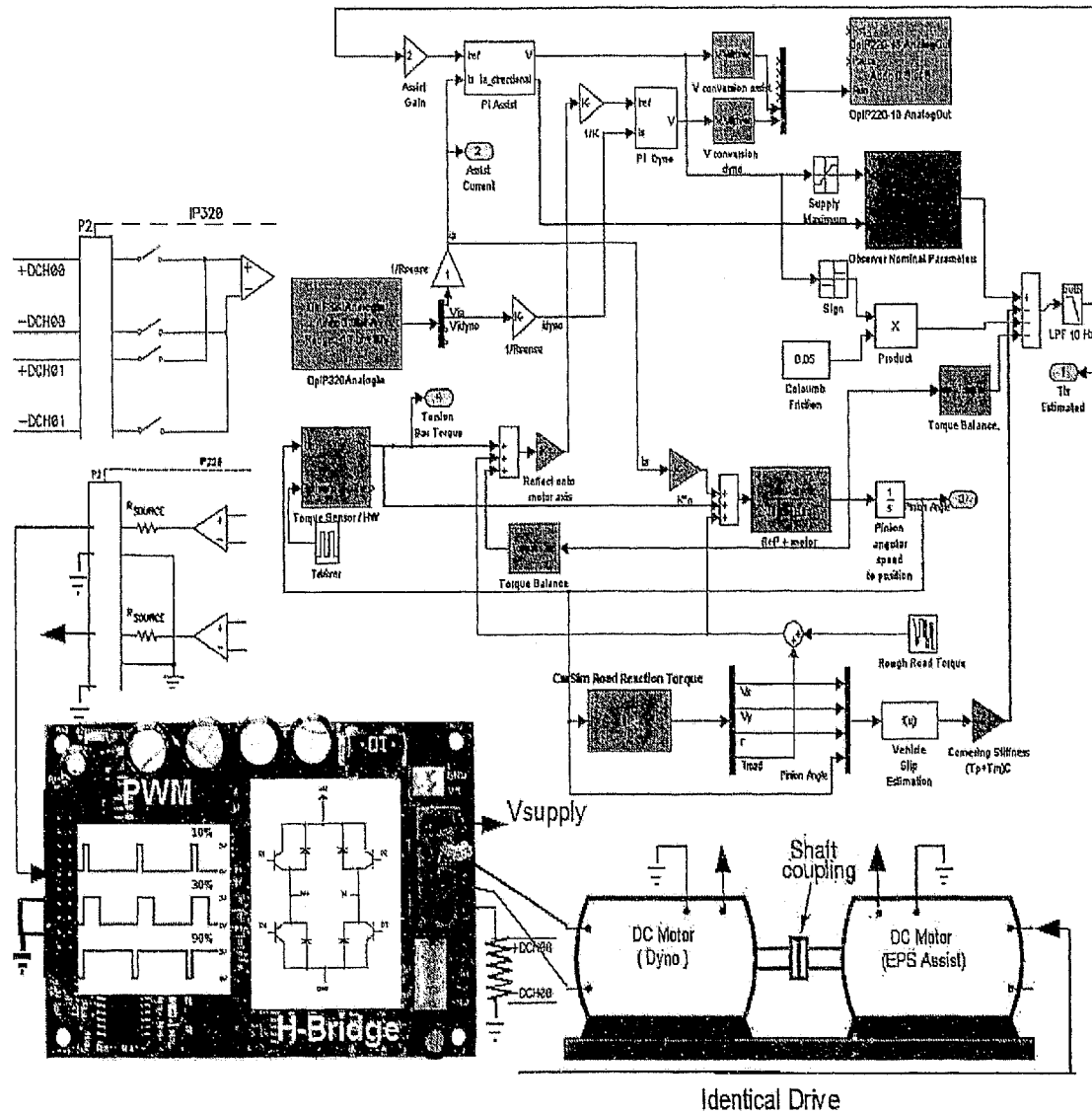


Figure 4.17: Hardware and Software Configuration for FTC of EPS

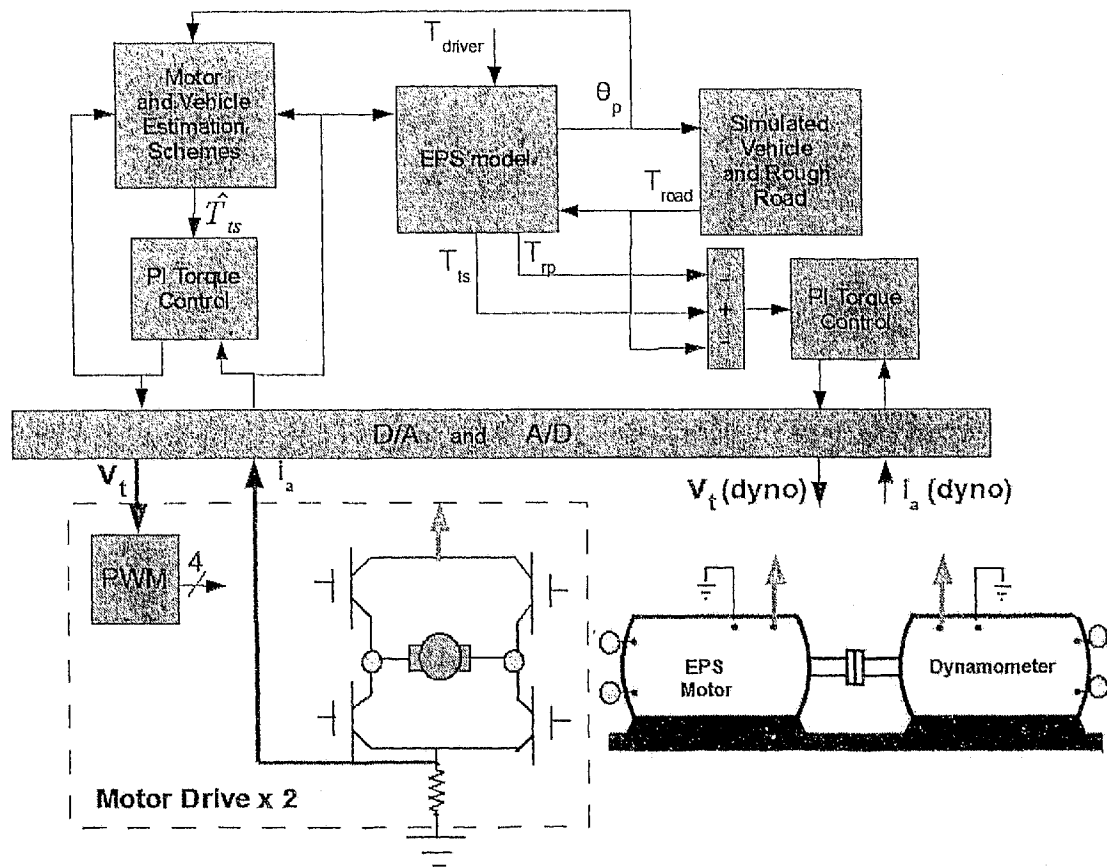


Figure 4.18: Block Diagram of FTC HIL Simulation setup

To demonstrate the Fault Tolerant Controller's validity in a realistic environment, CarSim™ is used to simulate the road torque due to the vehicle dynamics. The performance of the benchmark controller is compared to the Fault Tolerant Controller. The benchmark results are obtained based on the normal, torque sensor based control. In both cases, the vehicle input is a constant driver input torque of 5 second duration, then released, allowing the simulated vehicle to return to neutral steering position naturally.

#### 4.5 Determining Motor and Simulation Parameters

In the hardware results for the FTC scheme, the nominal motor model parameters for the observer are measured in separate experimental tests, as outlined in *Table 4.II*. These methods typically provide motor parameters within an accuracy of  $\pm 10\%$ , and reasonable performance is obtained, as seen by comparing *Figure 4.22* to *Figure 4.23*.

*Table 4.II: Determining Motor and Other Simulation Parameters*

Parameter	unit	How parameter is measured / calculated
$R_a$	$\Omega$	$R_a = \frac{V_t}{i_a}$ if $\omega_m = 0$
$L_a$	H	$\tau_e$ occurs when $i_a = 0.63 i_{a\_ss}$ $L_a = \tau_e R_a$ if $\omega_m = 0$
$K$	V / (m/s)	$V_t$ open circuit, $i_a = 0$ $K = \frac{V_{emf}}{\omega_m}$
$B_m$	s · N · m/rad	At steady state, $Ki_a = B_m\omega_m + K_f$ Linear regression, $y = mx + B$
$K_f$	N	“
$J_m$	s <sup>2</sup> · N · m/rad	$\tau_m$ occurs when $\omega_m = 0.63 \omega_{m\_ss}$ $J_m = \tau_m B_m$
$C_\alpha(t_p + t_m)$	N · m / rad	This value is approximated from the initial slope of the $\alpha_f$ versus $T_{align}$ curve provided in CarSim™, which is based on typical vehicle experimental data.

The motor armature resistance  $R_a$  can be measured either with an ohmmeter connected across the armature windings, or by applying Ohm's law to a blocked rotor and applying a constant known voltage. The armature inductance  $L_a$  can be estimated by measuring the electric time constant  $\tau_e$ . This is the time it takes for the motor current to build up to a

steady state value in response to a step voltage input, under blocked rotor conditions, in order to avoid the effects of back EMF. The motor flux constant  $K$  can be identified by operating the motor as a tachometer (that is, measuring the EMF voltage and rotational velocity with the armature windings open circuited). The motor dry friction  $K_f$  and viscous friction  $B_m$  can be measured by applying various constant voltages to the motor armature winding, and waiting for the motor to develop a constant torque and speed. This measures the motor's friction performance at different steady state operating points. Afterwards, linear regression is performed on the measurements. The motor's inertia  $J_m$  can be calculated by measuring the mechanical time constant  $\tau_m$  and with knowledge of the previous measured friction parameters. For purposes of this simulation, the signals  $V_x$ ,  $V_y$ , and  $r$ , as well as the vehicle parameters  $a$ ,  $b$ ,  $t_m$ ,  $t_p$ , and  $C_a$  are provided by CarSim<sup>TM</sup>. In an actual EPS system, these could be estimated via methods similar to those in [22], as discussed in Chapter 1.



#### 4.6 Analyzing the Effect of Parameter Variations on FTC Scheme

The performance of the observer based FTC scheme is very near to the normal controller when the real motor parameters are close to those used in the observer motor model. However, the motor parameters can vary significantly from their original values. The average steady state estimation error of the motor observer or Kalman filter of *Section 3.1*, when utilized for fault detection only, is zero. This assumes there is no offset (variation from nominal sense resistance) in the current sensor. Dynamic errors are present until the estimated state converges to its true value; this convergence is accomplished by the predictor/corrector feedback structure of *Figure 2.10*. However, when the estimated state is used as an input to the motor torque control, the error dynamics of this estimation scheme interfere with the plant (EPS) operation. This is true in general for full state feedback control (i.e. LGQ), as well, where observers provide the states: when the system parameters vary from their nominal ones, the separation principle no longer strictly applies [37]. The system (EPS motor with observed torque fed forward to the motor torque controller) as a whole can be analyzed similar to a procedure found in [36]. The effect of the parameter uncertainty can then be analyzed by the movement of the eigenvalues of the overall system. Overall, as the parametric variation increases the steady state estimation error increases. This causes the effective steering assist gain  $G$  to decrease.

These effects are more intuitively described by analyzing the difference in system response under different operating conditions (various percent of parameter variation). To quantify the loss in estimation accuracy of the observer, the system of *Figure 3.12* is analyzed using SISO frequency response (Bode magnitude) and step response plots. In this case, the input is the driver's torque (1 Nm step) and the output is the motor current which follows the estimated torque sensor. To isolate the effect of the motor observer component, the road torque estimation is assumed accurate. *Figure 4.19* compares two cases: 1<sup>st</sup>, the nominal system parameters used by the observer are equal to the real motor parameters (green). In the 2<sup>nd</sup>, the observer parameters are offset by a percentage of their actual value (blue). As the real motor parameters are impossible to measure exactly and

due to the fact they do vary (albeit slowly with respect to the motor dynamics), this is an important aspect to consider.

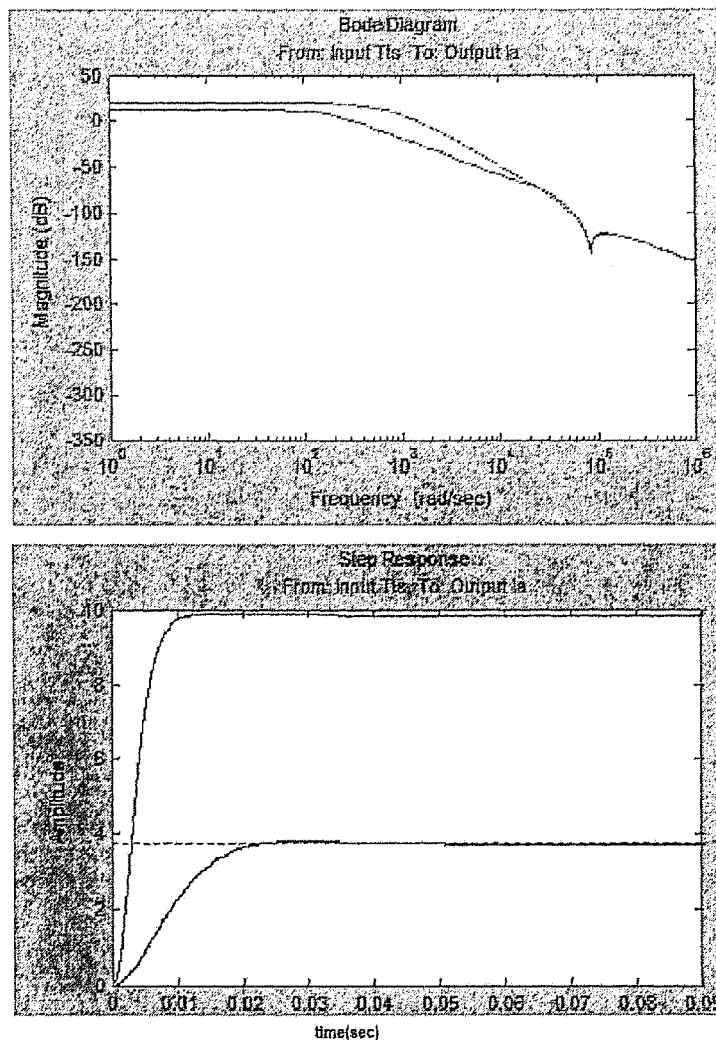


Figure 4.19: Frequency and Step Response of EPS subject to parametric variations

These particular plots use a gain  $G$  from torque sensor to current of 10 (so we expect a motor current of 10 A from the 1 Nm driver input). The lower traces (**blue**) are the case of each of the observer motor parameters being 40% less than the actual values. These parametric variations occur due to wear overtime, inability to measure the parameters accurately, manufacturing variance, etc. As can be seen from the step response plot (and inferred from the Bode magnitude plot), the current only reaches a value of just under 4A; hence, there is a 60% decrease in effective steering assist gain. This decrease

increases with greater parameter variations, as well as increases the greater the assist gain  $G$ . This causes an increasing demand for torque input from the driver to turn to the same steering angle. Otherwise, this does not drastically or detrimentally affect the steering torque assist performance (the case shown is an extreme case).

In addition, oscillation in the FTC scheme can be caused by:

$$R_{a \text{ observer}} > R_a \quad , \quad L_{a \text{ observer}} > L_a \quad (4-48)$$

and is avoided by choosing observer motor parameters marginally lower (10%) than those measured:

$$R_{a \text{ observer}} = 0.9R_{a \text{ measured}} \quad , \quad L_{a \text{ observer}} = 0.9L_{a \text{ measured}} \quad (4-49)$$

$R_a$  and  $L_a$  increase gradually overtime due to brush wear and as the temperature of the armature winding increases during periods of continuous current. Actual motor parameters that are larger than those used by the observer cause a decrease in steering assist gain as in *Figure 4.19*. This is certainly preferred to the case of the actual parameters being less than the observer's which causes increasing oscillation. Hence, observer parameters are chosen lower than their initial measured values as per *equation 4-49*. This causes a decrease in steering assist torque available, but will not cause oscillation or instability. A value of 10% is chosen to take into consideration inability to measure parameters exactly, manufacturing variance, etc. In this way, oscillation and instability is avoided when the motor is new and during its operational lifespan.

A detailed analysis of general frequency domain stability techniques, applied to state space methods (i.e. linear quadratic regulators and estimators) can be found in [37]. The system presented in this thesis is not covered specifically as it is not controllable; however, the examples in chapter 5 of [37] mirror the effects previously discussed. For the case of a state feedback controller where the states are delivered by an observer, the

effects of each can be separated and analyzed independently. However, this is not the case in face of parametric variations: the duality/separation principle no longer applies. The controller and estimator's ability to remain stable despite parameter variations is called *stability robustness*. Methods to improve the stability robustness of controllers and estimators designed using optimal and deterministic criteria are included. Alternately, mixed  $H_2/H_\infty$  approaches could be utilized to obtain similar results.

## 4.7 Results

Table 4.III: Summary of Experimental Assumptions and Settings

Variable	Setting
$V_x$	In CarSim <sup>TM</sup> the vehicle longitudinal velocity is 50 km/h.
$V_x, V_y, r$	These signals are provided by CarSim <sup>TM</sup> since it simulates the vehicle's dynamics.
$K$	The motor flux coefficient is assumed constant since the motor is operating in the non-saturated magnetic region.
$\alpha_f$	$\alpha_f < 4^\circ$ for the vehicle/tire set chosen in the simulation, which corresponds to driving inputs that keeps the vehicle stable.
$f_{PWM}$	=10 R/L, to produce a smooth motor current waveform.
$f_{sample}$	=1000 Hz, for model step and signal sampling.
$G$	The steering assist gain is set = 4 (since $K=0.25$ , this corresponds to a current demand equal to the torque demand).
$P_i$	The observer motor nominal parameters are set to: <u>Case 1:</u> 90% of the values as measured in <i>Table 4.II</i> . <ul style="list-style-type: none"> <li>• simulates normal controller settings</li> </ul> <u>Case 2:</u> 70% of the values as measured in <i>Table 4.II</i> . <ul style="list-style-type: none"> <li>• simulates a worn motor</li> </ul> <u>Case 3:</u> 90% of the values as measured in <i>Table 4.II</i> .
$T_{roughroad}$	This is generated by setting the peak magnitude of white noise signal on the pinion axis: <u>Case 1,2:</u> 0.1 Nm <u>Case 3:</u> 2 Nm
$T_{driver}$	4 Nm (steering wheel axis) for 5 seconds, then release.
$K_p, K_i$	PI torque control gains are tuned experimentally by setting the gains high enough to remove steady state error and obtain quick response / no overshoot, without causing ringing.
$f_{cutoff}$	The LPF cutoff frequency is set to 10 Hz. The filter order (# poles) is 20 in order to produce a sharp filter capable of effectively attenuating any high frequency estimated torque (13+Hz range).

*Figure 3.12* is simulated on the HIL setup of *Figure 4.17* with the settings shown in *Table 4.III*. To demonstrate the performance of the Fault Tolerant Controller in different conditions, three sets of results are presented. The 1<sup>st</sup> case simulates the motor and EPS assembly under new conditions with observer parameters set per *equation 4-49*. The 2<sup>nd</sup> case simulates the worn motor condition (increased parameters) by decreasing the observer motor model parameters to 70% of their measured values. Finally, in the 3<sup>rd</sup> case, the effectiveness of the controller in filtering out a higher amplitude rough road torque is shown. The benchmark control system, as simulated and shown in *Figure 4.20*, uses the actual (simulated) torque sensor signal for the motor torque control. The motor current and torque follow the torque sensor quickly with no steady state error, as a well tuned PI controller is used.

*Figure 4.22*, the 1<sup>st</sup> case, shows the FTC scheme under the same operating conditions (*Table 4.III*) as the benchmark controller. In the FTC scheme, the estimated torque sensor signal is used in lieu of the actual sensor. The ideal performance would be a system with identical performance as the fault-free system, but performance degradation is acceptable. Since the real motor parameters are subject to manufacturing tolerances, the methods for approximating them are reasonable (per *Table 4.II*). Using these approximate values in the motor observer, the torque sensor estimate has only approximately a 15% steady state error which causes a 15% decrease in steering assist torque. In terms of transient performance there is a slight lag (approximately 0.05 seconds) in the estimated versus actual (simulated) torque sensor signals.

In the 2<sup>nd</sup> case (*Figure 4-22*), the motor is simulated to be worn (increased parameters) by decreasing the values used by the observer. The resistance, inductance, flux constant, inertia and friction nominal values of the observer are decreased by 20%. In this case, there is an effective 40% decrease in steering assist torque.

In the 3<sup>rd</sup> case (*Figure 4-23*), despite there being a relatively high magnitude of rough road torque (2 Nm), little of this noise appears in the torque sensor estimate. This is due

to the sharp low pass filter (10 Hz cutoff frequency, 20 poles) applied to the torque sensor estimate.

These results show that the FTC scheme performs well under normal and more extreme operating conditions. This is reasonable performance for a fault tolerant controller in this application, since there would be *little perceivable difference between normal and fault tolerant controllers to the driver* besides a marginal increase in driving effort required to turn the wheels.

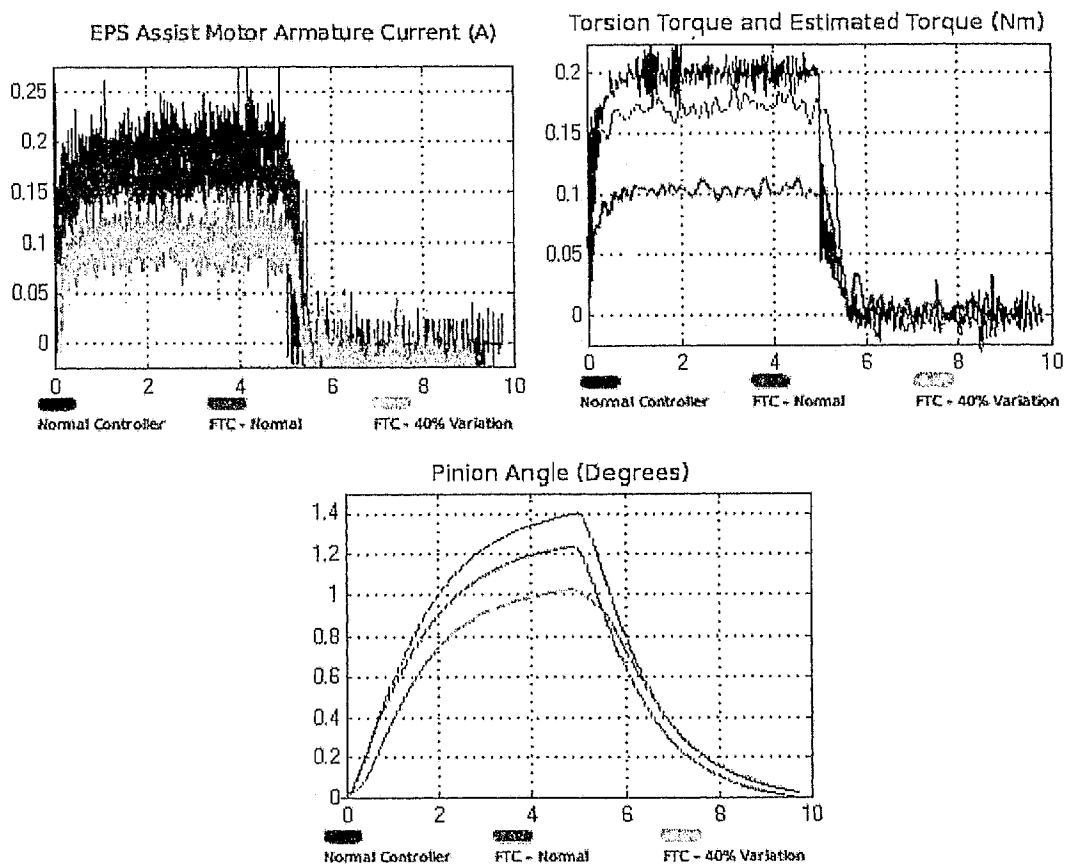


Figure 4.20: Comparison of FTC to standard controller

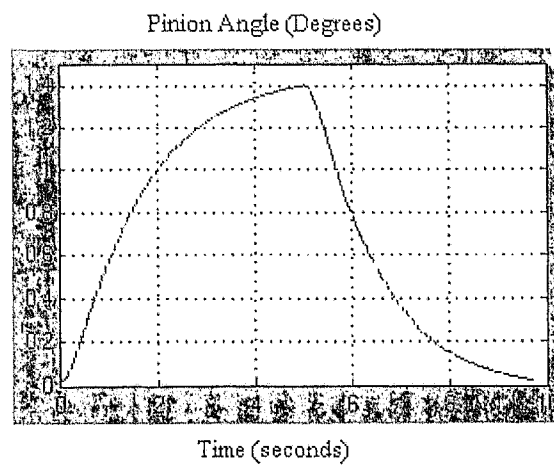
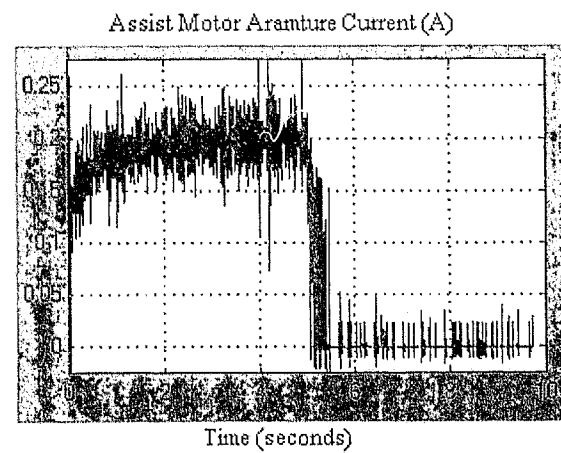
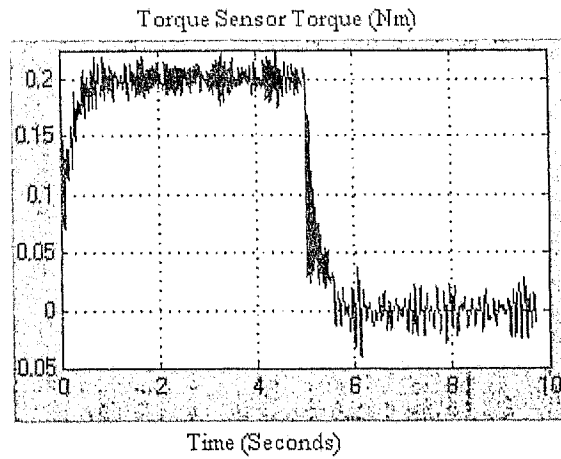


Figure 4.21: Normal EPS Controller - HIL Performance



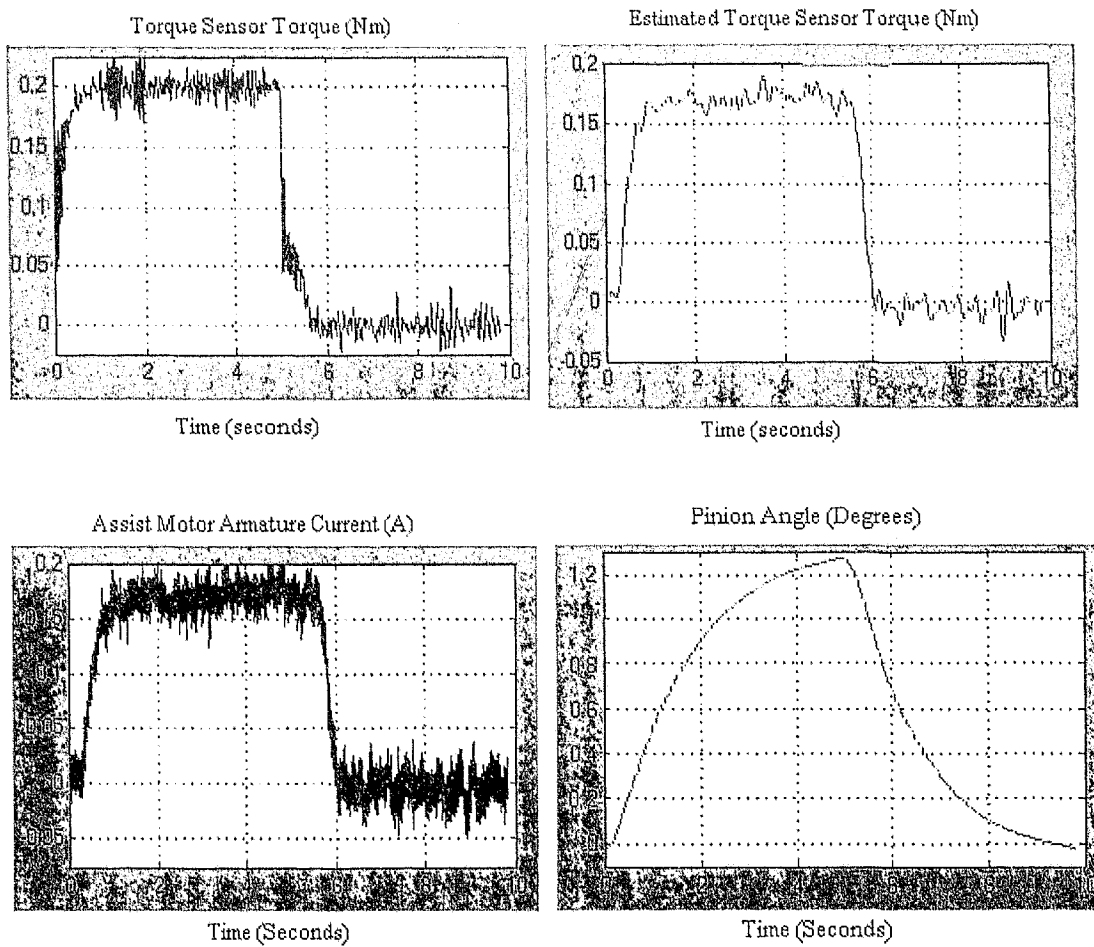


Figure 4.22: EPS FTC - HIL Performance, Nominal Observer Parameters

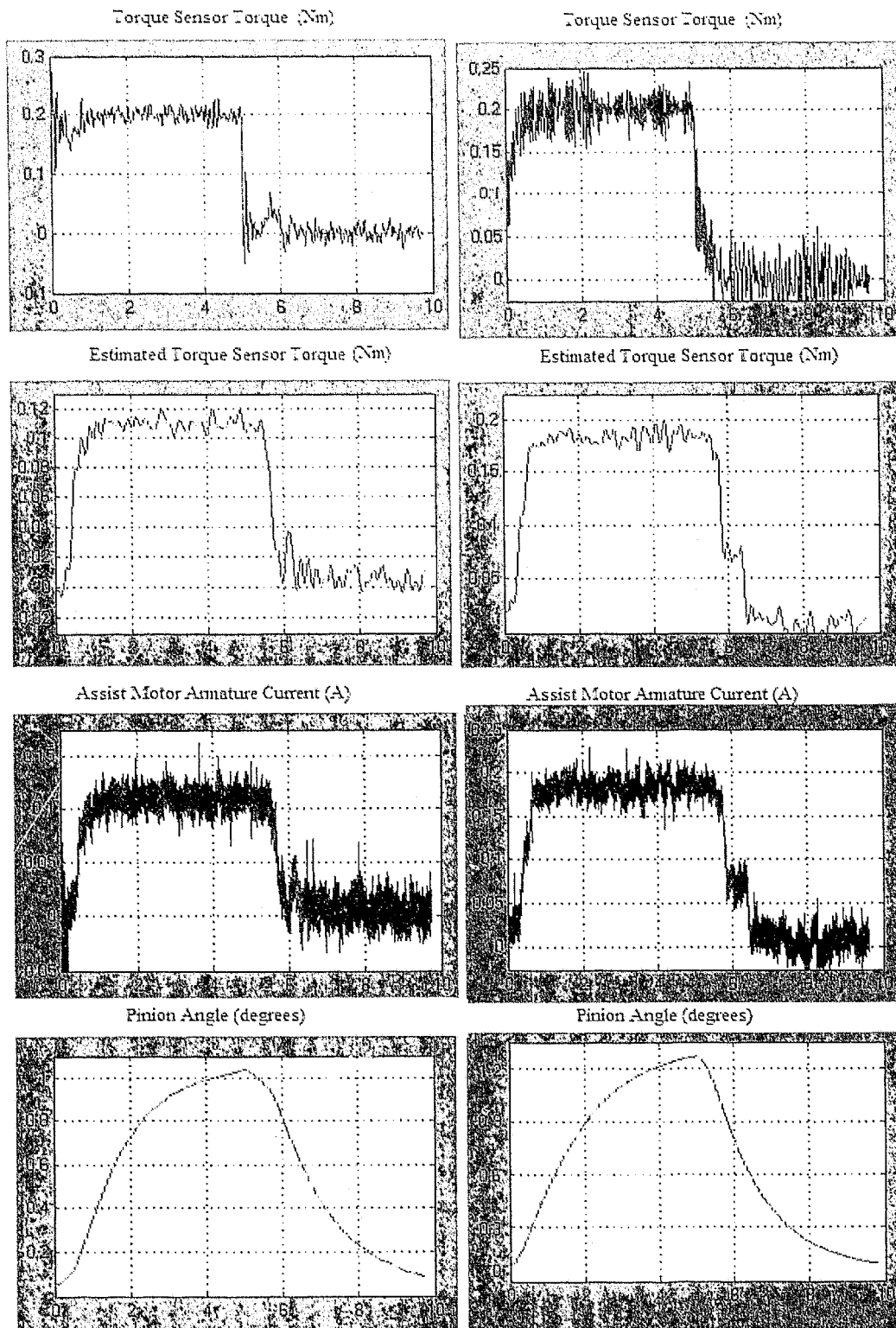


Figure 4.23: FTC Performance, 20% parameter variation

Figure 4.24: FTC Performance, Increased Road Roughness

## CHAPTER 5:

# CONCLUSIONS AND FUTURE WORK

### 5.1 Conclusions

An observer is designed to estimate the total disturbance torque on the motor axis, based on current/voltage measurements and the EPS motor subsystem model. An independent estimate of the road torque is obtained from a bicycle vehicle model and linear tire model, using input from sensors typically equipped in vehicle stability programs. The road torque is subtracted from the total disturbance torque in order obtain the torsion bar torque. The FTC scheme uses this estimated torque as a command to the DC motor drive, as a replacement for the torque sensor voltage output. High frequency rough road torques and signal noise are filtered out of the estimate using a sharp low pass filter.

The designed Fault Tolerant Controller uses no additional hardware, as no additional sensors are required. Since the observer filter gains are designed either using pole placement or steady states Kalman techniques, minimal real-time computational load is put on the microcontroller. Both the PI gains and filter gains are pre-computed; hence, only the 3<sup>rd</sup> order motor model need be computed in real-time. In general, having constant controller and estimator gains is only possible with linear systems: in non-linear systems, the system and associated gains are dependent on the magnitude of the input and output measurements.

A HIL simulation has been built to validate the ideas presented in this work. The simulation is setup to mimic real world driving conditions. The controller performs well in a variety of typical operating conditions, from worn components to very rough road surfaces. The degraded performance of the fault tolerant controller compared to the normal controller is a slight decrease in effective steering assist gain. This causes the driver to have to provide a somewhat greater share of the steering effort.

## 5.2 Future Work

For future work, an estimation scheme more robust to motor parameter variations could be designed, possibly by incorporating parameter estimation. One possible method is one similar to [42], which uses a model-adaptive approach in combination with a standard predictor-corrector estimator. In this way, the relative amount of steering assist torque would be more consistent. The practicality of this particular method is an open issue, however, and some sort of measurement of the shaft speed would be necessary. Adaptive control techniques are generally more difficult to tune, implement, analyze, and robustify compared to traditional single loop and state feedback controllers.

Besides improving the accuracy of the motor shaft torque estimate, a more accurate road aligning torque estimate may be needed in order for the Fault Tolerant Controller to be implemented in a real vehicle. For instance, instead of the linear tire model, the tire dynamics could be based on a full nonlinear model. Some higher fidelity tire models are vehicle speed dependant [43], which could extend the controller's range to work in driving conditions near and past the driving stability limit. Alternately, a more widely used model such as the HRSI tire model [23] could be utilized. These models take into consideration the cohesion friction between the road and tires which changes often depending on the driving surface, unlike the effective cornering stiffness and tire trail. Hence, this parameter would need to be identified in real time. ABS systems incorporate sensors and schemes which measure the tire/road friction coefficient which could be used for this purpose; alternately, a technique such as [22] could be used. This method uses linear and non-linear least squares parameter estimation techniques with measurement of the steering torque. Thus, the coefficient could only be updated in the EPS system when the torque sensor signal is available. Additionally, if needed, a higher DOF vehicle model could be used (i.e. a five DOF bicycle model [4]).

In this thesis, the prediction/corrector structure  $\hat{\mathbf{x}} = \mathbf{A}\hat{\mathbf{x}} + \mathbf{B}u + \mathbf{L}(y - \mathbf{C}\hat{\mathbf{x}})$  is used to estimate the disturbance torque on the motor. The prediction segment uses the linear system model and inputs to predict the values of the system states. The corrective term is

constructed by comparing the estimated current to the measured one. Each state estimate is corrected by multiplying this error signal by a filter gain  $\mathbf{L}$ .

Many approaches can be taken to design  $\mathbf{L}$ . Some designs lead to steady state gains, as in the case of the Luenberger/deterministic observer. On the other hand, the Kalman filter results in an algorithm with time-varying gains; however, if the projected error covariance  $\mathbf{P}$  reaches a steady state value, the gain  $\mathbf{L}$  rapidly reaches a steady state value as well. This steady state value of  $\mathbf{L}$  can be used in lieu of the time varying gain. The time varying gains require solving differential Riccati equations for each time step. Solving these equations requires matrix inversions, which can be difficult to compute in real-time, especially for higher order systems. However, the steady state gains can be pre-computed offline and stored in the microcontroller, with often negligible performance compared to the time varying counterpart. This results in little processing overhead on microcontrollers. Instead of the Kalman filter, a mixed  $H_2/H_\infty$  approach to design the state filter gains could be used. An example of such an approach using game-theory on the infinite time horizon is given in [39]. A discrete time version can be found in [40].

Irregardless of the design of the feedback gains  $\mathbf{L}$ , if the same predictor/corrector structure is used, the same resulting increase in steady state estimation error due to parametric variations will occur. Although the designed observers perform reasonably well in the cases presented in this thesis, a more robust solution would be ideal. That is, the observer and/or controller design criteria should result in a scheme more robust to state estimation error caused by model error. How to design such an estimation technique is the subject of future research.

An example of an alternate approach to disturbance torque compensation robustness is using a bank of Kalman Filters, each with different probable values of the system parameters. This is practical in the EPS motor case since a 3<sup>rd</sup> order LTI filter takes minimal storage on a microcontroller. A probability based decision scheme then picks the Kalman filter state output with the smallest estimation error covariance [44].

Furthermore, an overall robust fault diagnosis and management scheme could be developed for an EPS system by constantly monitoring the current signal, command voltage, position/speed signal (if any), and torque sensor. Typically, a combination of observer and parameter estimation techniques are used to generate residual signals. These signals are evaluated with decision making logic to determine if any of the sensors or actuators experiences a soft (drifting) or hard (failure) fault. Once the fault is isolated, a proper action can be taken. In some cases, it is possible to compensate for these errors with a fault tolerant controller in order to maintain performance in spite of a particular fault. For example, the FTC scheme developed in this thesis would be the action taken in the case of a diagnosed torque sensor failure. The developed observer could also be used to detect incipient or drifting faults.

## APPENDICES

### APPENDIX A

#### A. Glossary of Model Parameters and Control Variables

##### MOTOR DRIVE PARAMETERS

Parameter		unit	Value
$R_a$	Armature Resistance	$\Omega$	25
$L_a$	Armature Inductance	H	0.25
$K$	Flux Constant	V / (m/s)	0.24
$B_m$	Viscous Friction	s · N · m/rad	0.026
$K_f$	Coulomb Friction	N	0.05
$J_m$	Inertia	$s^2 \cdot N \cdot m/rad$	0.0065
$K_p$	Torque PI: Proportional Gain	$\Omega^{-1}$	50
$K_i$	Torque PI: Integral Gain	$\Omega^{-1}$	200

##### EPS AND VEHICLE PARAMETERS

Parameter		unit	Value
$B=B_{HW}$	Steering wheel dampening	s · N · m/rad	0.02
$J=J_{HW}$	Steering wheel inertia	$s^2 \cdot N \cdot m/rad$	0.033
$K_s$	Torque Sensor stiffness	N · m/rad	80
$B_s$	Torque Sensor dampening	s · N · m/rad	0.05
$B_{RP}$	Rack and Pinion Viscous Friction	s · N · m/rad	0.5
$J_{RP}$	Rack and Pinion Inertia	$s^2 \cdot N \cdot m/rad$	0.308
$n_s$	EPS motor gear Ratio	-	20
$n_s$	Effective Steering Ratio - pinion axis to wheel angle	-	16
$t_o=C_a(t_p+t_m)$	Cornering Stiffness * Tire Trail	N · m / rad	24,500

## REFERENCES

- [1] Aly Badawy, Jeff Zuraski, Farhad Bolourchi and Ashok Chandy; "*Modeling and Analysis of an Electric Power Steering System*"; SAE Technical Paper, 1999-01-0399, 1999.
- [2] N. Mohan, T. M. Uneland and W. P. Robbins; "*Power Electronics-Converters, Applications, and Design*"; 3rd Ed., John Wiley & Sons, 2003.
- [3] Paul Yih et al; "*Vehicle State Estimation Using Steering Torque*"; American Control Conference, 2004. Proceedings of the 2004, Vol.3, Iss., 30 June-2 July 2004
- [4] Taheri, S.; "*An Investigation and Design of Slip Control Braking Systems Integrated with Four Wheel Steering*"; Ph.D. Thesis; Clemson University, 1990
- [5] Xiang Chen and Xiaoqun Chen; "*Control-Oriented Model for Electric Power Steering System*"; Steering and Suspension Technology and Tire and Wheel Technology, SP-2019, 2006 SAE World Congress
- [6] Masahiko Kurishige and Takayuki Kifuku; "*Static Steering Control for Electric Power Steering*"; Mitsubishi Advance Technical Report, 2001
- [7] W. Burton Anthony; "*Innovation Drivers for Electric Power-Assisted Steering*"; IEEE Control Systems Magazine, Vol. 23, Issue 6, pp. 30 -39, 2003.
- [8] Shuji Endo and Hideyuki Kobayashi; "*EPS Control Technology*"; NSK Steering Systems Co; Motion & Control No. 16, August 2004
- [9] Isermann, R; "*Fault Diagnosis-Systems : An Introduction From Fault Detection to Fault Tolerance*"; Springer, 2006
- [10] Nicola Bianchi, Silverio Bolognani, and Michele Dai Pre; "*Design of a fault-tolerant IPM motor for electric power steering*"; Vehicular Technology, IEEE Transactions on, Volume 55, Issue 4, July 2006



- [11] Fuessel, D.; Isermann, R.; "*Hierarchical motor diagnosis utilizing structural knowledge and a self-learning neuro-fuzzy scheme*"; Industrial Electronics, IEEE Transactions on , vol.47, no.5. Dec.2001
- [12] Xiang-Qun Liu, Hong-Yue Zhang, Jun Liu, and Jing Yang; "*Fault Detection and Diagnosis of Permanent-Magnet DC Motor Based on Parameter Estimation and Neural Network*"; IEEE Transactions on Industrial Electronics, Vol. 47, No. , Oct 2000
- [13] Chee Pin Tan & Maki K. Habib; "*Tolerance towards sensor faults: An application to a flexible arm manipulator*"; International Journal of Advanced Robotic Systems, Vol. 3, No. 4 (2006)
- [14] RJ Patton; "*Fault-tolerant control systems: The 1997 situation*"; IFAC Symposium on Fault Detection Supervision and Safety, 1997.
- [15] Edwards, C.; Chee Pin Tan; "*Fault tolerant control using sliding mode observers*"; Decision and Control, 2004, CDC. 43rd IEEE Conference on, vol.5, no., pp. 5254-5259 Vol.5, 14-17 Dec. 2004
- [16] Campos-Delgado, D.U., Martinez-Martinez, S., Zhou, K.; "*Integrated fault-tolerant scheme for a DC speed drive*"; Mechatronics, IEEE/ASME Transactions on , vol.10, no.4, pp. 419-427, Aug. 2005
- [17] Matthew T. White, Masayoshi Tomizuka, and Craig Smith; "*Improved Track Following in Magnetic Disk Drives Using a Disturbance Observer*"; IEEE/ASME Transactions on Mechatronics, Vol. 5, No. 1, March 2000
- [18] Weiwen Wang, Zhiqiang Gao; "*A comparison study of advanced state observer design techniques*"; American Control Conference 2003, vol.6, no., pp. 4754-4759 vol.6, June 2003
- [19] Akinobu Sugiyama, Masahiko Kurishige, Hanako Hamada and Takayuki Kifuku; "*An EPS Control Strategy to Reduce Steering Vibration Associated with Disturbance from Road Wheels*"; SAE Paper 2006-01-1178
- [20] Jihan Ryu; "*State and Parameter Estimation for Vehicle Dynamics Control using GPS*"; PhD dissertation; Stanford University, December 2004
- [21] Stephant, J., Charara, A., Meizel, D.; "*Virtual sensor: application to vehicle sideslip angle and transversal forces*"; Industrial Electronics, IEEE Transactions on, vol.51, no.2, pp. 278-289, April 2004

- [22] Young-Hsiang Judy Hsu et Al; "*A Feel for the Road: A Method to Estimate Tire Parameters Using Steering Torque*"; 2006 Symposium on Advanced Vehicle Control (AVEC), Taipei, Taiwan
- [23] Dugoff, H., Fancher, P. S., and Segel, L.; "*An analysis of tire traction properties and their influence on vehicle dynamic performance*"; SAE Paper No. 700377.
- [24] Izumikawa, Y., Yubai, K., Hirai, J.; "*Fault-tolerant control system of flexible arm for sensor fault using reaction force observer*"; IEEE Transactions on Mechatronics, vol.10, no.4, pp. 391-396, Aug. 2005
- [25] C.R. Nave; "*Hyper Physics Concepts*"; tutorial website; <http://hyperphysics.phy-astr.gsu.edu/>
- [26] Akira Nogushi et Al; "*Development of Steering Angle and Torque Sensor of Contact-Type*"; Furuakawa Review, No.25, 2004
- [27] Didier Angleviel, Didier Frachon, Gérald Masson; "*Development of a Contactless Hall effect torque sensor for Electric Power Steering*"; SAE Paper 2006-01-0939
- [28] Ji-Hoon Kim, Jae-Bok Song; "*Control Logic for an electric power steering system using assist motor*"; Pergamon Mechatronics 12 (2002), pgs 447-459
- [29] Xiang Chen, Xiaoqun Chen and Kemin Zhou; "*Optimal Control of Electric Power-Assisted Steering System*"; Control Applications, 2005. CCA 2005. Proceedings of 2005 IEEE Conference, Aug. 2005, Page(s):1403 - 1408
- [30] Xiang Chen, Ke Li; "*Robust Control of Electric Power-Assisted Steering System*"; Vehicle Power and Propulsion, 2005 IEEE Conference, Sept. 2005
- [31] R.E.Kalman; "*A New Approach to Linear Filtering and Prediction Problems*"; ASME Transactions – Journal of Basic Engineering, Series D, pgs 25-45
- [32] L. Mcgee, S. Schmidt; "*Discovery of the Kalman Filter as a Practical Tool for Aerospace and Industry*"; NASA Technical Memorandum 86847, 1985
- [33] Various authors; "*MIT Open Courseware, Apollo Project Course*"; <http://ocw.mit.edu/OcwWeb/Science--Technology--and-Society/STS-471JSpring-2007/CourseHome>, accessed March 2008

- [34] Dan Simon; "*Optimal State Estimation*"; Wiley-Interscience, 2006
- [35] Seiichiro Katsura, Yuichi Matsumoto, and Kouhei Ohnishi; "*Modeling of Force Sensing and Validation of Disturbance Observer for Force Control*"; Transaction on Industrial Electronics, Vol. 54, No. 1, Feb. 2007
- [36] Giuseppe S. Buja, Roberto Menis, Maria Ines Valla; "*Disturbance Torque Estimation in a Sensorless DC Drive*"; IEEE Transaction on Industrial Electronics, Vol 42, No. 4; August 1995
- [37] R. Stengel; "*Optimal Control and Estimation*"; Dover Publishing, 1994
- [38] Wen-Hua Chen, Ballance, D.J., Gawthrop, P.J., O'Reilly, J.; "*A nonlinear disturbance observer for robotic manipulators*"; Industrial Electronics, IEEE Transactions on , vol.47, no.4, pp.932-938, Aug 2000
- [39] Xiang Chen and Kemin Zhou; " *$H_\infty$  Gaussian Filter on Infinite Time Horizon*"; IEEE Transactions on Circuits and Systems – 1: Fundamental Theory and Applications, Vol. 49, No. 5, May 2002
- [40] Ali Tahmesebi, Xiang Chen; "*Discrete-Time  $H_\infty$  Gaussian Filter*"; 2006
- [41] T. D. Gillespie; "*Fundamentals of Vehicle Dynamics*"; Society of Automotive Engineers, Warrendale, PA, 1996.
- [42] J.-S. KO, J.-H. Lee, M.-J. Youn; "*Robust digital position control of brushless DC motor with adaptive load torque observer*"; IEEE Proceedings of Electric Power Applications, Vol. 141, No. 2, March 1994
- [43] Hayama, R., Nishizaki, K., Nakano, S., Katou, K.; "*The vehicle stability control responsibility improvement using steer-by-wire*"; Intelligent Vehicles Symposium, 2000, Proceedings of the IEEE, Volume 1 , Issue 3 , 2000
- [44] T. Kobayashi; "*Application of a bank of Kalman filters for aircraft engine fault diagnosis*"; ASME Turbo Expo, Atlanata, paper GT2003-38550, June 2003.
- [45] P. Baracos, G. Murere, C. A. Rabbath, and W. Jin; "*Enabling PC-Based HIL Simulation for Automotive Applications*"; Technical Report, Opal-RT Technologies, Inc

- [46] Hui Li, Mischa Steurer, K. L. Shi, Steve Woodruff, and Da Zhang; "*Development of a Unified Design, Test, and Research Platform for Wind Energy Systems Based on Hardware-in-the-Loop Real-Time Simulation*"; IEEE Transactions on Industrial Electronics, Vol. 53, No. 4, Aug 2006
- [47] R. Isermann, J. Schaffnita and S. Sinsel; "*Hardware-in-the-loop simulation for the design and testing of engine-control systems*"; Control Engineering Practice, 7 (5), pp. 643-653,1999

## VITA AUCTORIS

NAME: Matthew Lawson

BIRTHDATE:

BIRTHPLACE: Windsor, Ontario, Canada

### EDUCATION

2005-2008

#### **Master of Applied Science**

*Electrical and Computer Engineering*

University of Windsor, Windsor, ON

- NSERC Canadian Graduate Scholarship

2001- 2005

#### **Bachelor of Applied Science (Honours Co-op)**

*Electrical and Computer Engineering*

University of Windsor, Windsor, ON

### RELEVANT WORK EXPERIENCE

2007- present

#### **Software Engineer**

*Link Testing Laboratories, Detroit, MI*

- Create custom software to meet Testing Requirements.
- Programs to retrieve and report dynamometer noise and performance data.
- Custom control and estimation techniques for dynamometer operation and post-test calculation.

2005-2007

#### **Graduate Teaching Assistant**

*University of Windsor – Electrical Engineering, Windsor, ON*

- Courses: EM Waves 1 and 2, C++, Control Systems.

2004

#### **Power Engineer (Co-op)**

*Ford Windsor Powerhouse, Windsor, ON*

- Conducted an in depth cost savings analysis of the steam turbine generator operation.
- Designed an electrical price monitoring program

#### **Electrical Engineer (Co-op)**

*Windsor Engine Plant – Engine Assembly, Windsor, ON*

2003

#### **Project Engineer (Co-op)**

*Ford Windsor Casting Plant, Windsor, ON*